IMPACTS OF BIOMASS BURNING AND LARGE-SCALE TRANSPORT ON THE SOUTHEAST ASIAN HAZE

Son Truong Cong Hoang

Department of Urban and Environmental Engineering

(Environmental Science and Engineering)

Graduate school of UNIST

2016

IMPACTS OF BIOMASS BURNING AND LARGE-SCALE TRANSPORT ON THE SOUTHEAST ASIAN HAZE

Son Truong Cong Hoang

Department of Urban and Environmental Engineering

(Environmental Science and Engineering)

Graduate school of UNIST

IMPACTS OF BIOMASS BURNING AND LARGE-SCALE TRANSPORT ON THE SOUTHEAST ASIAN HAZE

A thesis submitted to the Graduate School of UNIST

in partial fulfillment of the requirements

for the degree of Master of Science

Son Truong Cong Hoang

15. 06. 2016 Approved by

Major Advisor

Myong-In Lee

IMPACTS OF BIOMASS BURNING AND LARGE-SCALE TRANSPORT ON THE SOUTHEAST ASIAN HAZE

Son Truong Cong Hoang

This certifies that the thesis of Son Truong Cong Hoang is approved.

15. 06. 2016

Advisor: Myong-In Lee

Thesis Committee Member: Sung-Deuk Choi

Thesis Committee Member: Dong-Hyun Cha

Abstract

Biomass burning has significant impacts on regional air quality and climate in Southeast Asia. This study examines the impacts of biomass burning on the large-scale transport of aerosols and haze events using observational analysis and numerical model simulations. The spatiotemporal variation of observed aerosols shows significant correlations, positively with the emission induced by fire and negatively with the removal by precipitation both in seasonal and inter-annual timescale. Particularly, the variation of aerosol optical depth (AOD) retrieved from the Moderate Resolution Imaging Spectroradiometer (MODIS) is primarily affected by El Niño Southern Oscillation (ENSO), leading to a substantial year-to-year variation. The aerosol reanalysis data from the Modern-Era Retrospective analysis for Research and Applications 2 (MERRA-2) reveals that the aerosols emitted from combustion such as organic carbon and sulfate are the main contributors to the total AOD variation in this region. Organic carbon accounts for over 60 % of total AOD amounts, being highly correlated with the biomass burning, while sulfate also serves as a significant source for the background aerosol concentration. The impacts of aerosols on meteorology and the local air quality have been further investigated using the Weather Research and Forecasting/Chemistry (WRF-Chem) model simulations for June 2013 and September 2015. Overall, the model simulation can capture the most of observed spatial and temporal variations of aerosol appeared in MODIS and MERRA-2, although it tends to underestimate AOD for the both tested cases. The model sensitivity experiments show that both aerosol direct and indirect effects have significant impacts on meteorology and local air quality. The direct impact of aerosols tends to reduce the incoming shortwave radiation at the surface, thereby decreasing surface temperature and the planetary boundary layer (PBL) height. Because of decreasing the PBL height and stabilizing lower atmosphere, the aerosol direct effect tends to increase near-surface concentration of atmospheric trace gases such as NOx, CO and O_3. The indirect impact of aerosols also contributes to decrease the shortwave radiation through enhanced activation of cloud condensation nuclei particularly over the ocean. The near-surface concentration of trace gases tends to increase also by the aerosol indirect impact near the emission source except O_3, which actually decreases. In case of AOD and $PM_{2.5}$, both aerosol effects have significant impacts in which the direct effect increases AOD and $PM_{2.5}$ whereas aerosol indirect effect decreases AOD and $PM_{2.5}$. Although the direct and indirect feedbacks on aerosol mass concentrations are subject to uncertainties, this work demonstrates the significance role of aerosol feedback for real-time air quality forecasting under haze conditions.

List of Figures

List of Tables

I. Introduction

1.1. Background and Motivation

Nowadays, the global climate change is gaining more and more worldwide attention and becoming an important issues due to its consequences to the human civilization. As a result, the global climate change has largely affected spreading from global warming, polar glacier and sea-ice melting, increasing global sea surface temperature, and inflating the intensity of extreme weather phenomenon as well as its frequency such as the wildfire, typhoon, flooding across the globe. Throughout every part of the world, human being has vigorously impacted the environment and nature resource in many different pathways enclosing major anthropogenic activities contributed to global climate change such as production large combustion amount from fossil fuels, man-made deforestation and biomass burning. In recent decades, the biomass burning activities have gained more attention and been intensely researched because of its potentially dangerous contribution to human health as well as the global climate change. The term of biomass burning which may be referred as the slash-and-burn practice is associated with the activities of burning living plants, vegetation to remove crop residue and forests for the agriculture, plantations, and resettlement. Nowadays, it is becoming a common and regular methods as well as persistent activity in a number of tropical countries including Indonesia, Brazil, Mexico, etc (e.g., Aiken, 2004; Gadde et al., 2009; Gautam et al., 2013). In Southeastern Asia, the biomass burning event is usually happened in the Kalimantan and Sumatra provinces in Indonesia by plantation companies and developers (Tacconi & Vayda, 2006), with high intensity and fire peak from June to October during the dry season. The biomass burning is strengthening and intensifying during El-Nino Southern Oscillation (ENSO) years (e.g., Wang et al., 2004; Nichol, 1998). During the biomass burning process, large amount of smoke and haze is produced and transported to the nearby countries such Singapore, Malaysia, Philippines, or Vietnam and Thailand further northern direction, mostly due to the prevailing northerly winds during the inter-monsoon in Maritime continent. (e.g., Aiken, 2004; Heil & Goldammer, 2001). The abovementioned haze or so-called smoke plumes from biomass burning has resulted in the degradations of local and regional air quality (e.g., Vasconcelos et al., 2013b; Huang et al., 2013). In those regions, when the biomass burning occurs, it generates large amount of aerosol species and atmospheric traces gases which is immediately released into the atmosphere such as organic carbon (OC) which counts for largest proportion of aerosols during the biomass burning, black carbon (BC), and much more other aerosol species including sulfates, dust, nitrates, etc). Based on the IPCC (full name as Intergovernmental Panel on Climate Change), one of the most important factors that can change the earth's energy budget and cause the global climate change is the anthropogenic and natural elements and processes. In general, aerosol has serious impacts on air quality and climate not only affecting many

countries located in Maritime continent, particularly through the intercontinental transport of pollution but also impacts global scale.

At local scale, aerosol modifies atmospheric chemistry, affects socioeconomic and human health. The atmospheric aerosol species, particular matters, trace gases are playing significant influential roles the tropospheric chemistry (e.g., Permadi & Oanh, 2013; Chang et al., 2013; Okada et al., 2001). For instance, large amount of nitric oxide and hydrocarbons emissions released in the tropical regions during the biomass burring in dry season can intensify and increase the near-surface ozone concentration. Together with the biomass burning process, there is also large amount of carbon monoxide and methane produced which is directly taken part in the photochemical chemistry process and affected the oxidation efficiency when interacting with the hydroxyl radicals in the atmosphere. (Paul et al., 1990). Biomass burring process is a great source of different trace gases for the heterogeneous chemistry. Moreover, receiving large amount of solar radiation due to located nearby the equator as well as having high water vapor amount, the photochemical actives is high in the Maritime continent. The photochemical process is significantly important because of its ability to increase the second organic compound and second organic aerosol concentrations. Together with the primarily atmospheric trace gases, the second organic compounds also have large range of dangerous impacts to human health, local and regional climate, natural resource and ecosystems, air quality, earth's budget, etc. In local scale, biomass burning can greatly degrade the visibility to such an extent that can affect other life aspects such as impacts on socioeconomic development or even traffic safety. In a typical biomass burning, the visibility can be substantially reduced to less than 100 km (Wang et al., 2004). According to the economic reports in the haze event happened in 1997, the economic loss was estimated to be 8.9–9.7 billion USD (Barber. 2000). In addition, populations living in the regions has significant health problems and many potential risks due to degrade air quality during the biomass burning. As in 1997, estimated about 100 million people were exposed to the biomass burning and have acute health risk issues. In Indonesia, about 20 million people were estimated to have serious respiratory problems (Heil and Goldammer, 2001). Typically, respiratory problems (e.g. upper respiratory infections (URI)) and eye-related illnesses including bronchitis, asthma are the most potentially substantial direct health effects due to biomass burring. Aditame 2000 showed that number of URI patients reduces largely in accord with the reduced incidence of biomass burning. Associated with many potential immediate health risks, exposure to haze due to biomass burning also has long-term effect such as the micro-organic pollutants generated in the haze event can cause carcinogens, teratogens since it contains large amount of organic substances including ethylbenzene, benzene, phenol, etc) (Radojevic., 2003). Sastry, 2000 found that the polluted air contains hazardous substance which can increase the incidences of respiratory issues. Furthermore, Jayachandran, 2005 investigated the infant survival rates is decreased during the biomass burning in the long-term.

In regional scale, biomass burning influences the ecosystem and biogeochemical cycles. In Maritime continent, it has been increasing the frequency from 1970s (Heil & Goldammer, 2001), and become annual trans-boundary problem. In June 2013, as one of the biggest haze event, the air pollution index is records as highest in the past decade with large amount of emission happening in Singapore, Malaysia and further to other regions. Consequence, large amount of natural habitat has reduced, the local terrestrial landscape has been fragmented (e.g., Kobayashi et al., 2004; Cheyne, 2008; Yule, 2010). In addition, they can also interfere with the biogeochemistry process both in the ocean and land by changing the nutrients and chemical sources such as ion. The influence of haze on the regional scale to the atmospheric systems is apparent and direct (Brauer., 1998).

In global scale, aerosol changes cloud and precipitation and alters radiative energy balance. The earth's radiation budget can be alter due to aerosol interception in which the scattering and absorption process affects both long-wave and shortwave solar radiation (e.g., Ge et al., 2010; Seinfeld et al., 2004; Zhao et al., 2011). On the other hand, the aerosol species can act as ice nuclei or cloud condensation nuclei that can modify the cloud system and formation process through the aerosol indirect effect. (e.g., Haywood and Boucher, 2000; Satheesh and Moorthy, 2005). The first aerosol indirect effect is considered as the decrease of cloud droplet effective radius leading to enhance the cloud albedo and optical thickness. Hence, the second aerosol indirect effect is referred to as the reduction of precipitation efficiency and make long cloud lifetime in which enhances the cloud droplet concentration number and reduces the cloud droplet effective radius. Because aerosol species can act as ice nuclei and cloud condensation nuclei, so that it can influence precipitation efficiency and cloud properties (e.g., Zhao et al., 2011; Miller et al., 2004; Teller et al., 2012). Moreover, aerosols can potentially affect the atmosphere dynamics due to the radiative effects (e.g., Stanelle et al., 2010; Tompkins et al., 2005; Chaboureau et al., 2011). Additionally, the IPCC in its latest assessment report-5 stated that the greatest uncertainties in the anthropogenic impact on climate relate to aerosol particles.

The change in energy fluxes during 2011 relative to 1750 is quantifies as the radiative forcing. In the radiative forcing, the surface warming is defined as the positive radiative forcing and the surface cooling is defined as the negative radiative forcing. In this sense, the radiative forcing of the total aerosol effect which includes aerosol direct and indirect effects in the atmosphere is estimated of about -0.9 W m^{-2} in the range of -1.9 to -0.1 W m^{-2}. For the positive radiative forcing, most of its contribution is from the black carbon due to its ability in absorbing solar radiation whereas the rest of other aerosols contributes to negative radiative forcing. Even though aerosol effect process is well-known, the sign and magnitude of those processes are still unclear. However, aerosol species and its interception with cloud have substantially impacted on the global mean radiative forcing with high certainty.

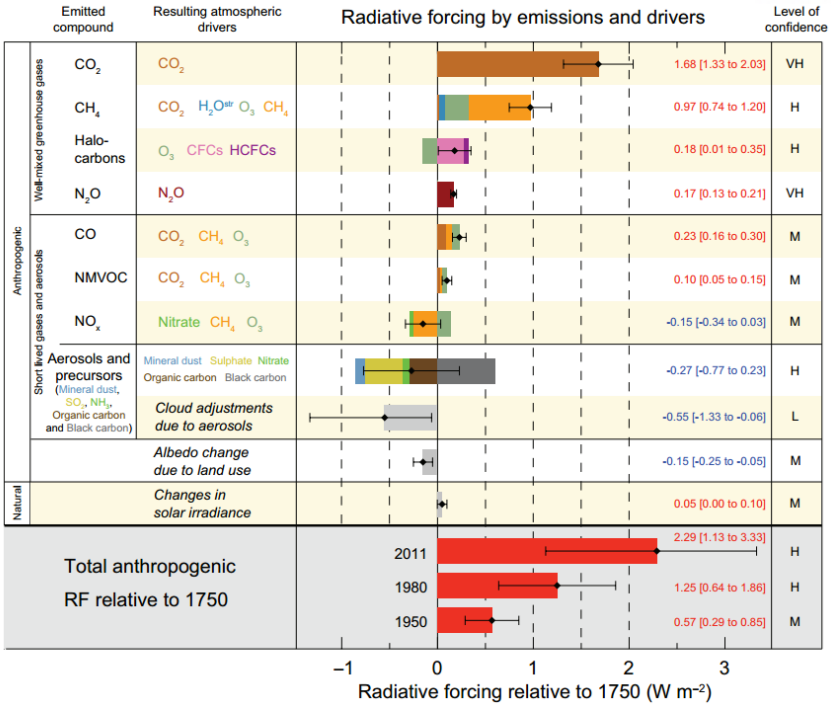

Figure I-1. The global radiative forcing and uncertainties for the main atmospheric species with the confidence level estimated of 2011 relative to 1750, (source: IPCC 5th Assessment Report – 2013)

In an aspect of global climate change contributed by all greenhouse gases, the total anthropogenic aerosol radiative forcing is estimated of about 2.29 in a range of 1.13 to 3.33 W m^{-2} for 2011 relative to 1750 (see Fig. 1). Furthermore, it has enhanced more quickly since 1970 compared to the prior decades. The radiative forcing of total atmospheric trace gases including N_2O, CH_4, CO_2, and halocarbons is about 3.00 in range of 2.22 to 3.78 W m^{-2} (see Fig. 1). In the concentration aspect, its radiative forcing change is about 2.83 in range of 2.26 to 3.40 W m^{-2}. In case of CO_2 itself, it can have a radiative forcing of 1.68 in range of 1.33 to 2.03 W m^{-2} (see Fig. 1). The emission of gases containing carbon attributing to the enhancement of CO_2 concentrations is estimated to have the radiative forcing of 1.82 in a range of 1.46 to 2.18 W m^{-2}. The radiative forcing of CH_4 itself is about 0.97 in range of 0.74 to 1.20 W m^{-2} (see Fig. 1). The other atmospheric gas species like carbon monoxide (CO) is essentially confident to induce a positive radiative forcing, whereas nitrogen oxides (NO_x) are more likely to induce a net negative radiative forcing.

1.2. Literature Review

In view of the above aerosol impacts, numerous efforts and researches have been carried out to understand and predict impacts of atmospheric trace gases, particular matter and aerosol species on atmospheric composition and global climate by integrating multiplatform (ground-based, balloon-borne, air-borne, ship-borne and satellite-borne) observations with mathematical models. Recently, the

Weather Research and Forecasting model coupled with chemistry (referred as WRF-Chem) is becoming a tool of interest for atmospheric community user. WRF-Chem has been largely employed to address the significance of man-made aerosols (e.g. anthropogenic) in regulating the local and regional climate alteration due to the aerosol effects (e.g. direct and indirect). Liu (2015) investigate the anthropogenic aerosol direct and indirect effect on meteorology and air quality in for months January, April, July, and October standing for four seasons in 2008 for East Asia. The results indicates that the aerosol effects caused by anthropogenic aerosol can decrease the surface shortwave radiation, 2m temperature, NO_2 photolytic rates and planetary boundary layer height to 40.5 – 57.2 W m^{-2}, 0.5-0.8ºC, 0.06 – 0.1 min^{-1}, and 83.6 – 130.4 m, respectively. The contribution of anthropogenic aerosol to its total number concentration is about 6.2 – 8.6x10^4 cm^3. Furthermore, the result also reveals that anthropogenic aerosol also increases the column cloud number concentrations to 3.6 – 11.7 x10^8 cm^2 and cloud optical thickness to 19.8 – 33.2. However, the daily precipitation over East Asia during the four months is almost reduced with the average amount of 3.9 – 18.6 mm. The haze event also simulated by Gao (2015) over North China Plain in January 2010. The results reveal that the PBLH is reduced up to 278.2 m and $PM_{2.5}$ concentration is enhanced over 20 μg m^{-3} in case of the aerosol feedback is included in the simulation. Furthermore, Zang (2015) investigated the aerosol effects in which the aerosol direct effect causes decreasing of the surface shortwave radiation flux, 2 m temperature, 10 m wind speed and the PBLH by 84.0 W m^{-2}, 3.2ºC, 0.8 m s^{-1}, and 268 m, respectively. Interestingly, in the simulation, the impact due to the aerosol indirect effects is relatively smaller even testing with finer grid of 9 km nested domain or replace the microphysics scheme from Lin to the two-moment Morrison scheme. Furthermore, the aerosol direct and indirect effects enhance the surface concentrations of primary trace gases such CO and SO_2 due to reducing the PBLH and stable the low atmosphere. Surface O_3 mixing ratio is decreased by 6.9 ppb because of decreasing the incoming surface solar radiation and lower temperature. The work emphasizes the important of including the aerosol feedbacks for simulating and predicting the real-time air quality forecasting during the haze event. Although WRF-Chem model contributes to understand the scientific point of aerosol impacts, it still has high uncertainty. Difference in the chemical and aerosol modules using in the model option can results in various different simulation output. In general, the uncertainties in emission inventories together with its temporal, spatial, vertical distribution, meteorological simulation, model coarse grid resolution, chemical reaction process, aerosol formation, etc are all contributed to large model biases for chemical concentrations (Liu et al., 2015, Zhang et al., 2015). One of interesting work contributed by Jena (2015) that compare different anthropogenic NO_X emission inventories and investigate the difference in modeling the near-surface surface ozone concentration in India during summertime from 15 March to 15 April and wintertime from 01 December to 31 December, 2005.

The research was carried out by applying the six different anthropogenic NO_X emission inventories including Indian National Emission Inventory (India_NOx), Emission Database for Global Atmospheric Research (EDGAR), MACCity, Regional Emission Inventory in Asia (REAS), Top-Down NO_X emission inventory for India (Top – Down) and the Intercontinental Chemical Transport Experiment-Phase B (INTEX-B). OMI satellite observations is used for comparison, the results showed that using the REAS emission inventory, the model reproduces tropospheric NO_2 columns with largest bias of $-243.0 \pm 338.8 \times 10^{13}$, the next uncertain emission inventory is the EDGAR emission inventory with $-199.1 \pm 272.2 \times 10^{13}$, followed by the MACCity emission inventory with $-150.5 \pm 236.3 \times 10^{13}$, INTEX-B emission inventory with $-96.8 \pm 199.5 \times 10^{13}$, India_NOx emission inventory with $-87.7 \pm 159.9 \times 10^{13}$ and Top-Down emission inventory with $-30.8 \pm 69.6 \times 10^{13}$ inventories. As the results of difference in simulation NO_X concentration due to different emission inventories, the model tends to reproduces different 8-h averaged ozone concentration with maximum deviation of 9 – 17 ppb which accounts for 15 – 40% in the summertime and 3 – 12 ppb which accounts for 5 – 25% in wintertime. The study indicates that the selection of NO_X emission inventories have significant influence in the simulated near-surface ozone concentration and other atmospheric trace gases. Despite the fact that WRF-Chem has applied in various places around the world, there is not much studies and researches have been implemented in the Southeast Asia region where anthropogenic aerosol and atmospheric trace gases due to biomass burning have been increasing dramatically over the last decade. In this perspective, some efforts have been carried out to understand the influence of biomass burning in Southeast Asian on the regional and global atmospheric composition and on climate by conducting intensive field campaigns. From August and September of 2012, an international intensive field campaign called Studies of Emissions and Atmospheric Composition, Clouds and Climate Coupling by Regional Surveys (SEAC4RS) used multiple aircrafts to study the influence of biomass burning and pollution (e.g. investigate the distribution of atmospheric trace gases due to deep convection in the troposphere), its spatial distribution and temporal evolution, and influence on local and regional meteorological processes as well as its feedback to regional air quality (e.g. the impacts and feedbacks of aerosol species due to biomass burning and man-made aerosol on regional meteorology and climate based on the changes in energy budget (aerosol direct effect) or the changes in clouds (aerosol indirect effects)). Additionally, another field campaign called the Seven Southeast Asian Studies (7 SEAS) program conducted from 2008 – 2013 (Reid et al., 2013; Lin et al., 2013). The main purpose of the campaign is to examine the influence of aerosol generated from biomass burning to atmospheric radiation, hydrological cycle, microphysics cloud, finally its impacts on regional climate. The campaign is carried out including many countries such as Thailand, Indonesia, Philippines Malaysia, Vietnam, Singapore, Taiwan, and the USA. Lawrence (2001) used Division of Atmospheric Research Limited Area Model (DARLAM: semi-Lagrangian regional climate model to simulate wind trajectories and

Particular Matter dispersion for researching on the transport of haze event generated during the big biomass burning in 1997. Generally, DARLAM quantified haze transport and emphasis fire-related biomass burning important, but still limited at what factors modulate the haze (e.g. climate variability, El-Nino, monsoon) and analyzed aerosols (e.g. BC, OC, AOD…). Engling (2015) applied Hybrid Single-Particle Lagrangrian Integrated Trajectory (HYSPLIT) to find Mass balance of typical TSP (e.g. BC, OC). Classically, these offline models does not allow the online interactive feedback between the aerosol and meteorological variable so that short-term atmospheric processes which needs the interaction between aerosol and meteorology can be missed (Forkel et al., 2012). Recently, Aouizerats (2015) implemented Weather Research & Forecast coupled Chemistry using Global Fire Emissions Database (GFED: and found that AOD is still underestimated. All the regional models qualitatively reproduced the patterns of surface ozone with higher levels over the Maritime Continent. However, due to the insufficiency of measurements and satellite observations, investigating of the spatial distribution of aerosol impacts and atmospheric trace gases in Southeastern Asia is still remaining a challenging task. Scientifically, it is become more and more difficulty for understand and explain the processes and underling mechanisms of natural phenomenon.

1.3. Research Objectives

In light of current conditions as addressed above, it is necessary to carry out more detail research to investigate the impacts of aerosol due to the biomass burning. The present thesis is aimed at establishing the credibility of a newly developed next generation fully coupled WRF-Chem over the Southeastern Asian region and use the model to understand regional distribution and variability of summertime AOD. The summer season is chosen because biomass burning loading over this region is highest in this season. Our research on Southeastern Asia is necessary, with fire emission due to biomass burning and trans-boundary haze increasing in the last decades. The objectives of this study will be covered as follows:

a) Characterizations of SEA Haze: A quantitative assessment of spatiotemporal aerosol variability based on long-term observations
b) Evaluation of the simulation capability by atmospheric chemistry/aerosol transport model
c) Understanding of aerosols feedbacks on regional meteorology and air quality

The thesis includes of four chapters including this introductory chapter. The WRF-Chem model configuration is presented in Chapter 2 together with the emission inventories, chemical and meteorological initial and boundary condition. Chapter 3 presents the assessment of the model performance using different statistical metrics, evaluates against ground-based observations, satellite retrievals and the reanalysis fields. The important findings are summarized in Chapter 4 along with the future research plans in this area.

II. Data and Model Experiments

2.1. Study Area

The Southeast Asia is located on Maritime Continent which is mostly defined with latitude spreading from –10 °S – 20 °N and longitude spreading from 90°E – 150°E. The region is including many countries such as Indonesia, Malaysia, New Guinea, Philippine, Singapore, Vietnam, etc and geographically located between the Pacific Ocean and Indian Oceans. The climate type in the region is mostly contributed by the interaction between the land and ocean. The typical Southeast Asia map is shown in the Fig. II-1 as follows:

Figure II-1. Southeastern Asia (Source Google Earth)

Based on the averaged prevailing wind in the Maritime continent, the weather is typically divided into 4 different types: the first is the northeast monsoon season which usually occurs from December to early March, the second type is the inter-monsoon period which occurs from late March to May, the third type is the southwest monsoon season which usually occurs from June to September, and the last one is the inter-monsoon period which mainly occurs from October to November. During the main four periods, the transition among them is relatively slow and gradual, happen every two months. The wind are usually strong and distinct during the northeast and southwest monsoon season whereas it is relatively light and inconsistent in the other two periods.

The Maritime continent plays an important roles in the earth's climate system. It is known as the indo-pacific warm pool where the sea surface temperatures is always higher than 28°C especially during the El-nino years. It is also known as the warmest oceans around the global as warm water mostly

contributed by the easterly trade winds towards western pacific. Due to its high sea surface temperature, the ample moisture is enhanced and creating the unstable atmospheric environment favoring for the development of deep convective typhoon and storms, even at daily scale. During this process, there is large amount of energy transfers to the upper-atmosphere and transports to the west and east direction as Walker circulation.

2.2. Observational and Reanalysis Data

2.2.1. Satellite-borne Observations

The MODIS (Moderate Resolution Imaging Spectroradiometer) is used to measure radianaces at the top of the atmospheric at various spatial resolutions (1000m, 500m, 240m) through 36 channels spreading from 0.41 μm to 14 μm. The MODIS satellite instruments includes two specific sensors which are Terra and Aqua, both are observing from the polar orbit. The Terra and Aqua have operated since February 2000 and June 2002, respectively (King et al., 2003). The aerosol retrieval data from MODIS is different between the ocean and land (Kaufman et al., 1997, Tanre et al., 1997) in which the aerosol retrieval over ocean is more accurate (Remer et al., 2005) compared to the land. The detail algorithms and description for aerosol retrieval process as well as its information is provided in the website link http://modis-atmos.gsfc.nasa.gov (Levy et al., 2010). In our study, both MODIS Terra and Aqua sensor v5.1 L2 is used daily for retrieving the aerosol parameter.

For the precipitation data, the Global Precipitation Climatology Project (GPCP) data is used for validation. This data is developed by the Laboratory for Atmospheres at the NASA Goddard Space Flight Center. It includes global precipitation data. The GPCP data is provided in a daily and monthly package with high resolution, available from 1979-present combined observations and satellite data into 2.5°x2.5° global grids, global precipitation data.

2.2.2. Aerosol Robotic Network Data

The Aerosol Robotic Network (AERONET) was developed by the National Aeronautics and Space Administration (NASA) (Holben et al., 1998). It is a ground-based remote sensing aerosol network with over 1000 monitoring sites currently. The AERONET measure aerosol optical properties by using the sun- and sky-scanning radiometers (Dubovik and King, 2000). AERONET provides columnar aerosol optical depths at a specific gridded point and can be located both in land or ocean (Alam et al., 2011 and 2014a). The AERONET instrument was intensely tested and proved to be reliable and continuous data on measuring aerosol optical depth even restricted in a single gridded point value (Dubovik et al., 2000). In this study, the AERONET v.2, level 2 cloud-screened and quality assured AOD at 500 nm from seven sites. At each AERONET station, single gridded point value retrieved will be compared with single gridded point model simulated value. These six sites are Bandung (6ºS, 107ºE, 826 m),

Jambi (1ºS, 103ºE, 30 m), Palangkaraya (2ºS, 113ºE, 27 m), Pontianak (0ºN, 109ºE, 2 m), Singapore (1ºN, 103ºE, 30 m), and Kuching (1ºN,110ºE, 28 m).

2.2.3. Reanalysis Data

The Modern-Era Retrospective analysis for Research and Applications 2 (MERRA-2) is a NASA atmospheric reanalysis currently being produced with the GMAO/GEOS-5 Data Assimilation System Version 5.12.4. MERRA-2 consists of fully modeled and analyzed aerosol fields in which it allows the feedback between aerosol and meteorology. The Goddard Chemistry, Aerosol, Radiation, and Transport model (GOCART) integrated into the Goddard Earth Observing System Model, Version 5 (GEOS-5) modeling system. These MERRA wind components are available at 1h, 3h, daily, monthly data and upto present at the spatial resolution of resolution of 0.5° lat x 0.625° lon x 72 hybrid sigma/pressure levels. Products variables simulated by GOCART such as OC, BC, Sea salt, dust, sulfate; Aerosol precursors (CH3, SO2), CO, etc.

2.3. Model Experiments

2.3.1. The WRF-Chem Model Description

The Weather and Research Forecast coupled with Chemistry is currently developed by the NOAA, DOE/PNNL NCAR, and other research group communities. The model firstly developed by Skamarock et al., 2008 (http://www.mmm.ucar.edu/wrf/users/) and it is a non-hydrostatic and fully compressible model. The Morrison double-moment scheme is used to represent the resolved scale cloud physics (Morrison et al., 2009). The WRF-Chem model encompasses a variety of single and double moment schemes to explicitly resolve water vapor, clouds and precipitation processes. The double moment schemes predict mixing ratios of these variables along with the number concentrations while the single moment schemes also predict only the number concentrations of prognostic species of water (e.g. ice, rain, snow, cloud, and hail). The prediction of both mixing ratios and number concentrations allows for a more robust treatment of the particle size distributions. Therefore, the double moment microphysical parameterization described by Morrison et al. (2009) has been used here. The model allows online interaction between meteorology and aerosol by using the Rapid Radiative Transfer Model (RRTM) (Mlawer et al., 1997), which is represented how shortwave and longwave transfers in the atmosphere. The RRTM mainly provides the atmospheric heating process which is generated by surface downward radiation, surface longwave radiation and radiative flux divergence. The longwave radiation part contains the thermal radiation and infrared radiation which is resealed and observed from the surface ground, aerosol, and trace gases. The near-surface upward longwave radiation emitted from ground is the emissivity which is calculated based on the land use, land cover types, or other parameters like temperature. In cased of the near-surface upward shortwave radiation, it is the amount of reflection because of surface albedo. In this scheme, both shortwave and longwave radiation respond to chemical

trace gases, aerosol such as nitrate, sulfate, carbon monodioxide, ozone and to the water vapor as well as cloud simulated by model.

The land-surface models utilize the atmospheric information from the surface layer scheme, radiative forcing from the radiation scheme and precipitation forcing from the microphysics and convective schemes, together with internal information on the land's state variables and land-surface properties to provide the heat and moisture fluxes over land points and sea-points. These fluxes provide a lower boundary condition for the vertical transport done in the PBL schemes. The MM5 similarity scheme and NOAH Land Surface model are used to represent the model surface process. The land-surface models utilize the surface layer scheme to get the atmospheric background, the radiation scheme for radiation forcing, and the convective and microphysics schemes for precipitation forcing. The other parameters on moisture and heat fluxes on land and ocean is provided by the land-surface properties. In order to allow the vertical sub-grid scale eddy transport, the Yonsei University (YSU) boundary layer scheme is employed (Hong et al., 2006). Therefore, the explicit vertical diffusion process in the model is deactivated immediately after the activation of the PBL scheme and the PBL scheme is assumed to handle this process. Several parameters such as moisture, horizontal winds and temperature are nudged with nudging coefficient of 6×10^{-4} s^{-1} in all vertical levels.

The Model for Ozone and Related Chemical Tracers (MOZART-4) chemical scheme is employed as the gas-phase chemistry in simulation (Emmons et al., 2010). The scheme is designed to represent the tropospheric chemistry of different chemical environments ranging from remote to polluted regions. The mechanism includes 4 inorganic intermediates, 17 inorganic species, and 32 organic species with 4 of them being of biogenic origin and 24 organic intermediates participating in total 237 reactions. The Model for Simulating Aerosol Interactions and Chemistry – MOSAIC (Zaveri et al., 2008) is used to represent the aerosol processes. The MOSAIC scheme simulated the bulk aerosol mass, converted into assumed modal distributions and divided into four size bins to allow for interaction among MOSAIC aerosols and radiation (e.g. direct aerosol effect, effect on photolysis) or interaction with clouds (indirect aerosol effect, aqueous chemistry, wet removal).

In order to provide the chemical background conditions for model simulation, the MOZART-4 (Emmons et al., 2010) is employed as it provides the initial and lateral boundary conditions available every six hour. The anthropogenic emission inventory is taken from EDGAR-HTAP in which a number of non-methane volatile organic compounds (NMVOC), chemical trace gases and aerosol are provided such as NO_x, SO_2, NH_3, black carbon, carbon monodioxide, and organic carbon. The fire emission inventory for emissions of atmospheric trace gases due to biomass burning is taken from NCAR for daily data.

The Model of Emissions of Gases and Aerosols from Nature is used to provide the atmospheric trace gases, aerosol due to biogenic emissions. The Wesely (1978) is used to parameterize dry deposition of atmospheric trace gases. Additionally, the Neu and Prather (2012) is employed to describe the washout of atmospheric trace gases. Both the washout through convective precipitation and grid-scale consider the same atmospheric trace gas species with the same Henry's law constants.

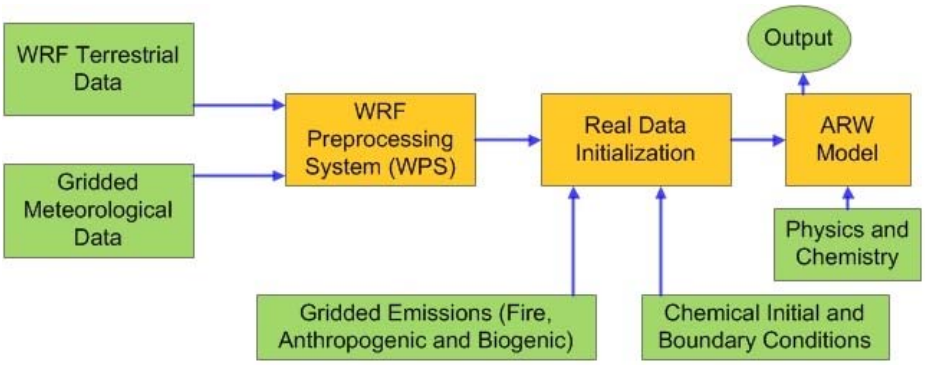

Figure II-2. Major components and flow chart of the WRF-Chem Modeling System specific to this study. The light green boxes represent the external data to the model system while the light orange boxes represent the major components of the modeling system.

WRF-Chem model is composed mainly of three components as portrayed in Fig. II-2. These components are (i) the preprocessing program (WPS), (ii) real data initialization program and (iii) the WRF solver including ARW and NMM coupled with chemistry. These components are described in detail in the following subsections along with external datasets used as input.

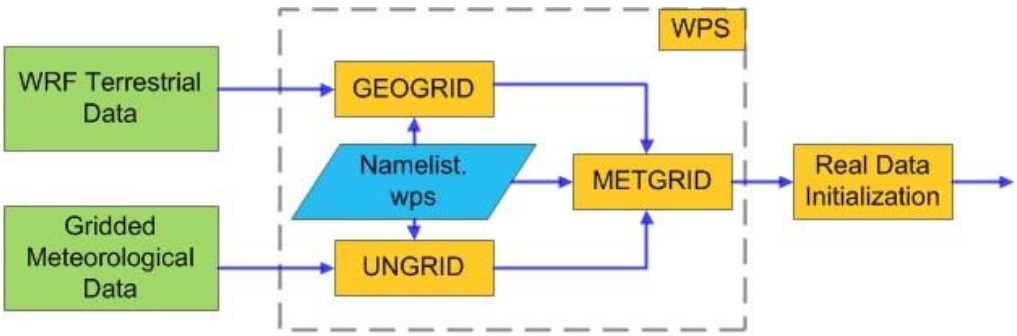

Figure II-3. Major Components of the WPS are shown along with the data flow among these components

The main objective of the WRF Preprocessing System (WPS) is to prepare input meteorological data for next step, i.e. for real data initialization program. WPS is composed of a set of three programs known as (1) geogrid, (2) ungrib and (3) metgrid. The study domain and terrestrial data of its domain is interpolated by the geogrid program while the ungrib program extracts the meteorological data from the gridded binary (GRIB) format and writes the data into an intermediate format. Both output from geogrid

and ungrib processes are used for metgrid program, then interpolates intermediate meteorological data horizontally onto the simulation domain. The data flow among three components of WPS is shown in Fig. II-3.

The interpolated metgrid output as generated from above process is now ready for use by the real data initialization program. The real data initialization program of the WRF-Chem model can also be segregated into two parts. The first part deals with the initialization of the model with the meteorological fields and static terrestrial data available in the WPS output, while the second part deals with the preparation of emissions and initialization of models with the chemical fields.

2.3.2. Model Configuration

The Weather Research and Forecasting Model v3.6.1 coupled with Chemistry is applied to examine the aerosol impacts on meteorology and air quality over Maritime continent (Fig. II-1). The Mercator projection is applied in this study with the longitude extending east-west from 90º – 130º E (including 150 total grid points) and latitude extending north–south from –10º – 20º N (including 120 total grid points). The model horizontal resolution is of 30 × 30 km^2. There are total 27 vertical levels from surface to 10 hPa. In Maritime continent, the study domain includes various different types of topographic condition, landscape, rainforests, as well as seashores. The model used United States Geological Survey (USGS) data at resolution of 10 min (~ 19 km) to interpolate the static geographical fields such as soil properties, terrain height, vegetation fraction, etc. The different and complex terrain in Maritime continent due to rapid change between land and ocean topographic can have an impact on local and regional meteorology as well as the distribution of chemical trace gases. The National Center for environmental Predictions (NCEP) Final Analysis (FNL) field data provides the initial and lateral boundary conditions for the meteorological fields which is obtained every 6 h with resolution of 1º × 1º. The model configuration is summarized in below table.

Table II-1. Summarize the characteristics of the three scenarios.

Attribute	Model configuration
Simulation period	June 2013, September 2015
Initial condition and boundary condition	NCEP FNL, provided every 6 h with spatial resolution of 1º x 1º
Longwave radiation	The rapid radiative transfer model (RRTM) (Mlawer et al., 1997)
Shortwave radiation	Goddard shortwave radiation scheme (Chou and Suarez, 1994)
Microphysics	Morrison double-moment scheme (Morrison et al., 2009)
Cumulus Physics	Grell-3D (Grell and Devenyi, 2002)

Planetary boundary layer	Yonsei University (YSU) PBL scheme (Hong et al., 2006)
Fire Inventory	Fire Inventory from NCAR (Wiedinmyer et al., 2011)
Aerosol Process	Model for Simulating Aerosol Interactions and Chemistry (MOSAIC) (Zaveri et al., 2008)
Biogenic emissions	Model of Emissions of Gases and Aerosols from Nature (MEGAN) version 2.04 (Guenther et al., 2006)
Anthropogenic emission	EDGAR HTAP emission inventory 2010
Gas-phase chemistry	Model Ozone and Related Chemical Tracers (MOZART-4) (Emmons et al., 2010)

The model simulation periods include two discrete times which are 01 – 30 June, 2013 and 01 – 30 September, 2015. For the first simulation, the model simulation started on on 29 May 2013 at 00:00 UTC and finished on 30 June 2013 at 23:00 UTC. In the second simulation, the model simulation started on 26 August 2015 at 00:00 UTC and finished on 30 September 2015 at 23:00 UTC. Model outputs hourly in both cases. The spin-up time will be 3 – 5 days, and model output from first day for the month to the last day of the month will be used for further analysis.

In the model simulation for meteorology, the model is re-initialized every 5 days based on the NCEP – FNL data whereas the chemical information is continuously obtained and processed from the previous simulation. Model's results with output data started at 01 June 2013 to the last day of the month is used for further analysis, and the first three days are discarded as a spin-up time. The reason for selecting the 2013 case because 2013 was a year with no major climate anomalies (no major ENSOs), but exceed 1997-98 records. (SO_2, PM_{10}, $PM_{2.5}$, NO_2, CO and O_3) (David et al., 2014; Jin et al., 2015, Erik et al., 2015); for the 2015 case, it was an extreme year of El-Nino and caused extreme worst haze conditions (e.g. air quality, living, economy).

The model uses various sources of pollutant chemicals and aerosols at surface. The anthropogenic emission is specified by the HTAP_V2 dataset, which consists of 0.1º x 0.1º grid maps of many different atmospheric trace gases and pollutant such as NMVOC, NH_3, PM_{10}, $PM_{2.5}$, BC, CH_4, CO, SO_2, NOx, and OC. The HTAP_V2 emission inventory is constructed based on the nationally reported emissions together with the regional inventories. This emission inventory are the joint corporation of a number of scientific including EMEP/TNO, the REAS, US-EPA, the EDGAR and the MICS-Asia to use for the purpose of researching the hemispheric transport of air pollution.

The Model of Emissions of Gases and Aerosols from Nature (MEGAN) is used to online provide aerosol and atmospheric trace species generated by biogenic emissions (Guenther et al., 2006). The isoprene emissions are calculated using spatial maps of isoprene emission factors while emission factors for other species are assigned according to the plant function types. The information about the spatial

distributions of isoprene emission factors, plant function type leaf area index, surface temperature, etc available at website link http://www.acd.ucar.edu/wrf-chem/.

The Fire Inventory from NCAR (FINN version 1) is used to provide the daily data emission of aerosol as well as atmospheric trace gases generated during the biomass burning (Wiedinmyer et al., 2006, 2011). Fire locations over the simulation domain are identified using MODIS Terra and Aqua derived Fire and Thermal Anomalies Product (Giglio et al., 2006). The fuel loadings for the pixels showing fire activity are determined by using global land cover dataset that provide the vegetation types, land use and percentage vegetative covers. The combustion efficiency for the herbaceous and woody fuels for each pixel is determined by using the methodology developed by Ito and Penner (2004).

2.3.3. Sensitivity Experiments

For each year in this study, there are 3 simulations as in the following table:

Table II-2. Model validation scenario

Case name	Short-name	Characteristics
No – Fire simulation	No-Fire	Without FIRE Inventory
FDDA simulation	FDDA	With FIRE inventory and FDDA
Control simulation	CTR	With FIRE Inventory and without FDDA

Those are WRF-Chem without fire emission inventory (No-Fire), WRF-Chem simulation with “Fire” using Four-Dimensional Data Assimilation (FDDA) and the WRF-Chem simulation with “Fire” and without FDDA. To examine the influence of including aerosol feedbacks in model simulation to meteorology and air quality, there are three WRF-Chem simulation with “Fire” and without FDDA scenarios are carried out and analyzed. The first simulation is named the control simulation (CTR), does not include any aerosol effects on meteorology (e.g. indirect and direct). The second simulation (EX1) deals with the radiative effects by adding the aerosol direct effect to the CTR simulation. The third simulation (EX2) includes all aerosol effects on meteorology by adding the aerosol indirect effect to the EX1. Regardless of the differences in the aerosols effects, the three simulations are identical in other input data such as emission inventory, fire inventory, initial and boundary conditions) or model setup. Finally, the difference between EX2 and CTR simulation (EX2 − CTR) is used to examine the impact of total aerosol feedbacks. On the other hand, the difference between EX2 and EX1 (EX2 – EX1) and that between CTR and EX1 (EX1− CTR) stands for the impacts of the aerosol indirect effects and direct effects, respectively. Following table summarizes the characteristics of the three simulation.

Table II-3. Aerosol impact investigation scenarios

Case name	Short-name	Characteristics
Control simulation	CTR	Without any aerosol feedbacks
Direct effect simulation	EX1	With aerosol direct effects
Indirect effect simulation	EX2	With all aerosol feedbacks

2.3.4. Evaluation Methods

In order to investigate model error and its performance ability in simulating the meteorological and chemical variables, there are a number of different statistical methods being used including mean bias (MB), root mean square error (RMSE), coefficient of determination (r2), and prediction error (E). Firstly, the prediction error is calculated as the difference between the observed and simulated values as follows:

$$\mathbf{E} = (\mathbf{O_i} - \mathbf{M_i})$$

To examine model bias which is the overestimation and underestimation of variable to the observation data, the mean bias is calculated as follows:

$$\mathbf{MB} = \frac{\mathbf{1}}{\mathbf{N}} \sum_{\mathbf{i=0}}^{\mathbf{N}} (\mathbf{O_i} - \mathbf{M_i})$$

In equation above, M_i and O_i stand for the i^{th} modeled and observed values, respectively. The total are summed of total number of model-observations pair values (N).

Linear relationship between model and observations is defined based on the coefficient of determination (r^2) and the correlation coefficient (r) is calculated as

$$\mathbf{r} = \left[\frac{\sum_{\mathbf{i=1}}^{\mathbf{N}} (\mathbf{O_i} - \bar{\mathbf{O}})(\mathbf{M_i} - \bar{\mathbf{M}})}{\sqrt{\sum_{\mathbf{i=1}}^{\mathbf{N}} (\mathbf{O_i} - \bar{\mathbf{O}})^{\mathbf{2}} \sum_{\mathbf{i=1}}^{\mathbf{N}} (\mathbf{M_i} - \bar{\mathbf{M}})^{\mathbf{2}}}} \right]$$

In equation above, the over bars over O and M stand for average observation and model value. The RMSE counts for error compensation due to inverse sign differences and is calculated as:

$$\mathbf{RMSE} = \sqrt{\frac{\sum_{\mathbf{i=1}}^{\mathbf{N}} (\mathbf{O_i} - \mathbf{M_i})^{\mathbf{2}}}{\mathbf{N}}}$$

III. Results and Discussion

3.1. Observed Characteristics of Aerosol Variability

The AOD variable, precipitation and fire radiative power are obtained from the MODIS monthly data with resolution of 1° x 1° (available 2000 to the present), from Global Precipitation Climatology Project (GPCP) data (available 1979 to the present) and from MODIS Fire Pixel data, respectively (available 2000 to the present). The following Fig. III-1 presents the annual map of fire count, AOD, and precipitation averaged during 2001 – 2015. It be seen that high intensive fire was frequently occurring in Sumatra and Borneo, Indonesia. Together with this high fire occurrence is the high AOD values in those regions. In Maritime continent, specially, the fire regions such Sumatra and Borneo, the wind commonly flows from the south or southeast direction between June and October and from north or northeast direction between December and early March.

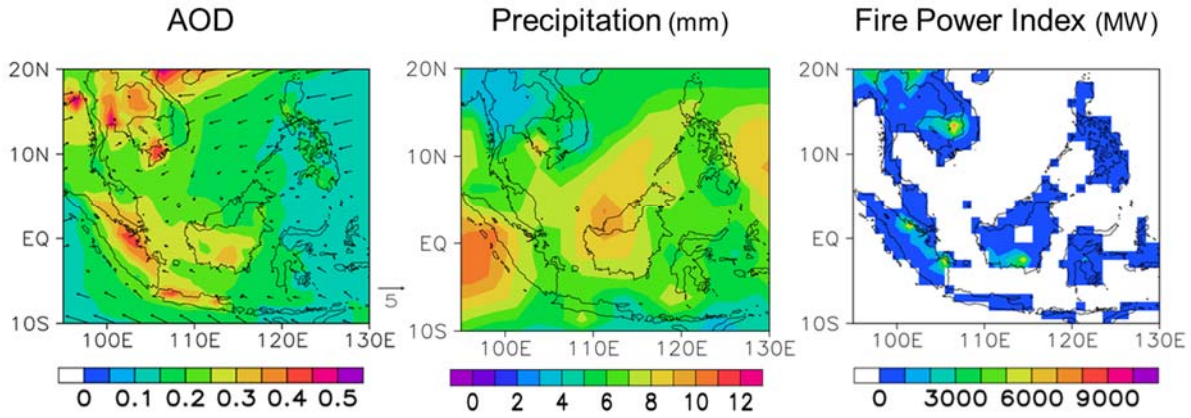

Figure III-1. Spatial distribution map of annual averaged aerosol optical depth, precipitation, and fire power index during 2001 – 2015 (left to right)

In order to understand the characteristic of AOD, precipitation, and fire, Fig. III-2 presents the seasonal cycles map during 2001 – 2015 for each season including the winter (DJF), the spring (MAM), the summer (JJA) and the autumn (SON). It is noticeable that most of high AOD value usually occurs in the south of the study domain during the JJA and SON period whereas high AOD value is high during DJF and MAM in the north of the study domain. One of the main reason for this high fire occurrence can be due to the impacts of the seasonal monsoon which contributing to shorten the precipitation during June to October each years. In June, the wind in Maritime continent reverses due to the cold air moves towards Maritime continent from Australia. Therefore, Maritime continent region is influenced by the monsoon regime. The spatial distribution map shows that high AOD signal goes along with relatively low precipitation amount and high fire power index. This suggests high AOD, fire power index and low precipitation can be related to ENSO.

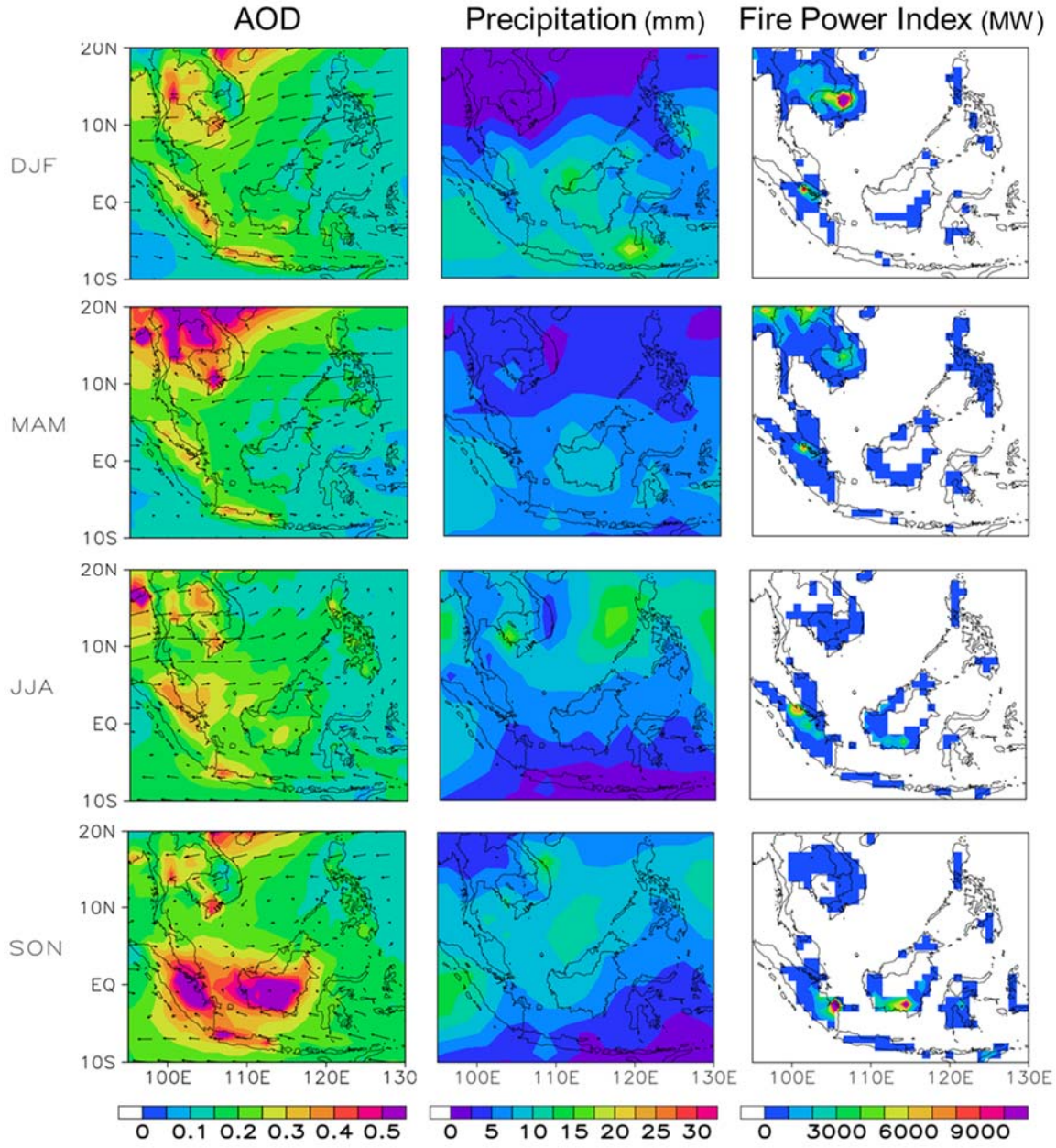

Figure III-2. Southeast Asia seasonal spatial distribution map of AOD, precipitation, fire power index in each season from 2001 – 2015

So as to pinpoint the interactive link of Fire, AOD, precipitation, the study domain is divided into 4 main regions namely: region I (95ºE-120ºE;-5ºS-5ºS) as the main center of the biomass burning; region II (120ºE-130ºE;-5ºS-5ºS) as the downwind region of the biomass burning; region III (95ºE-120ºE;10ºS-20ºS), Indochina region; and region IV (100ºE-115ºE;-10ºS-5ºS), industrial region. The time series of the averaged seasonal cycle value of each region during 2001- 2015 is plotted in Fig. III-3. The red, black, green lines present the Fire count, AOD and precipitation, respectively. In the left figure, each dot indicates the domain-averaged value of each month averaged over the entire period from 2001 to

2015 in each specific region. Firstly, there is a strong positive relationship between the fire count and AOD and negative relationship between precipitation and fire count in the seasonal cycle of AOD in region I, II, IV. It is apparent that the high intensive season of biomass burning usually happens in summer and repeats each years. The precipitation is almost totally out of phase compared to fire count and AOD values in those 3 regions. On the other hand, the tendency is opposite in region III, the figure indicates that most of the fire happens in the spring time with high AOD and low precipitation. However, it is so negligible fire occurrence and AOD value during the summer time compared to the region I, II, and IV.

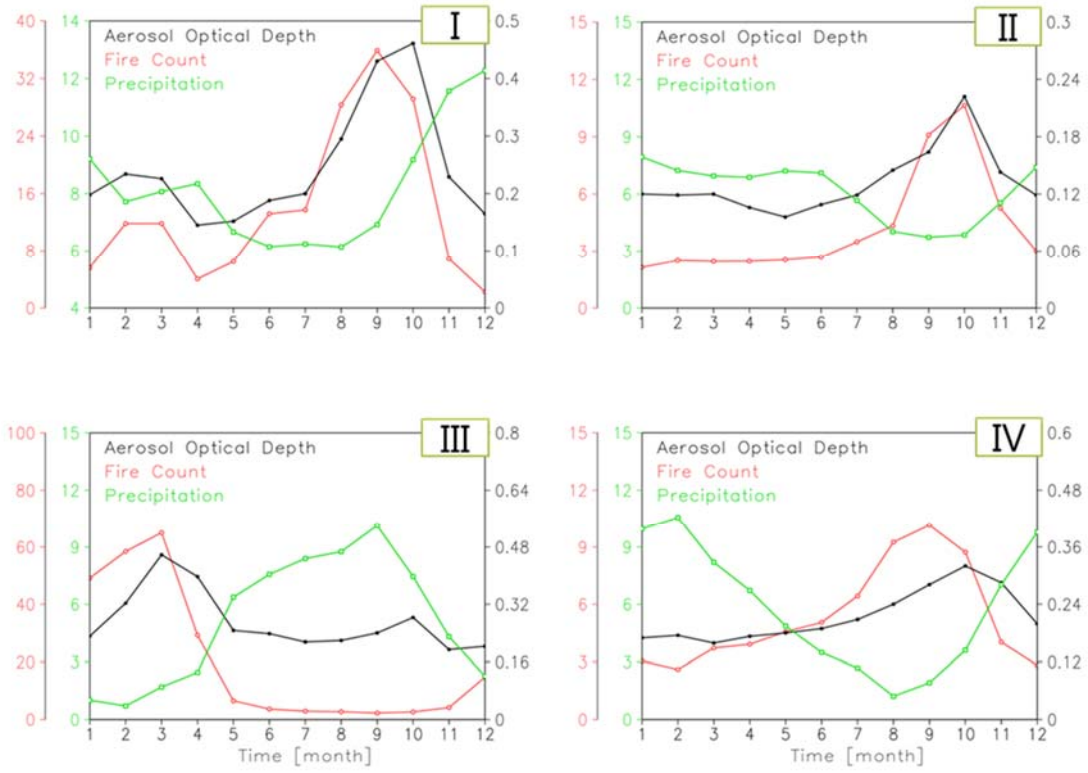

Figure III-3. Seasonal cycle of fire count, aerosol optical depth, and precipitation averaged in each region during 2001 – 2015

As presented in Table III.1, high positive correlation is found between AOD, Fire and negative for precipitation. For region I, the correlation is 0.91, -0.91 between fire and AOD, and precipitation and AOD. This indicates that the main source contributing to the AOD value is due to fire and the sink of AOD is due to precipitation.

Table III-1. Correlation of seasonal cycle of fire count, AOD, precipitation during 2001 – 2015

	Region I			Region II			Region III			Region IV		
	AOD	FIRE	RAIN	AOD	FIRE	RAIN	AOD	FIRE	RAIN	AOD	FIRE	RAIN
AOD	-	0.91	-0.91	-	0.94	-0.79	-	0.69	-0.46	-	0.71	-0.52
FIRE	0.91	-	-0.44	0.94	-	-0.86	0.69	-	-0.83	0.71	-	-0.89
RAIN	-0.09	-0.44	-	-0.79	-0.86	-	-0.46	-0.83	-	-0.52	-0.89	-

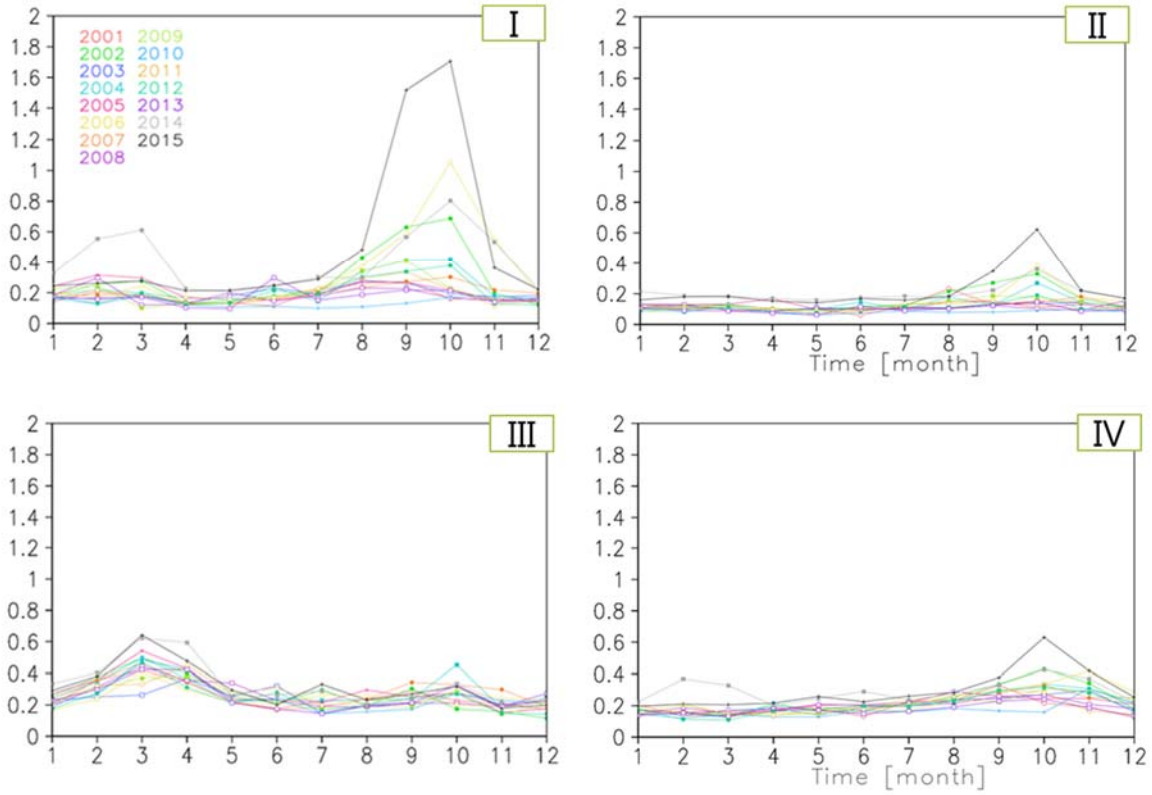

Figure III-4. Seasonal cycle of AOD each year (2001 – 2015)

Fig. III-4 shows the seasonal cycle of AOD. Each line presents the domain-averaged AOD value in each month at specific regions so that 15 lines associated with 15 years of 2001 to 2015 are presented. It can be seen that the AOD trend in the region I, II, and IV are similar in which the peak usually happens during the summer time and the opposite trend is found in region III, as the peak AOD is in the spring time as discussed above. The AOD seasonal cycle shows that there were a number of super-high AOD months in October, 2006, September and October 2015, etc. There were also other high peaks such as in October 2004, September 2009, and June 2013.

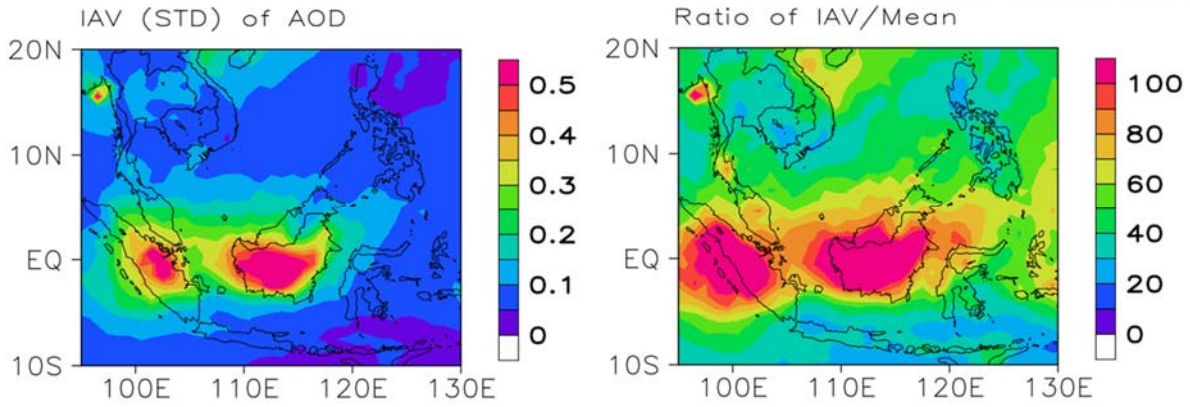

Figure III-5. Spatial Maps of IAV (STD) of AOD & the Ratio of IAV/Mean

Fig. III-5 shows the spatial maps of inter-annual variability standard deviation of AOD (left) and the ratio of inter-annual variability to the mean (right). It can be seen that high standard deviation is almost appearing in the biomass burning regions. The ratio with maximum value of 100% indicates that there is high fluctuation of AOD value suggested the role of ENSO in modulating the AOD intensity.

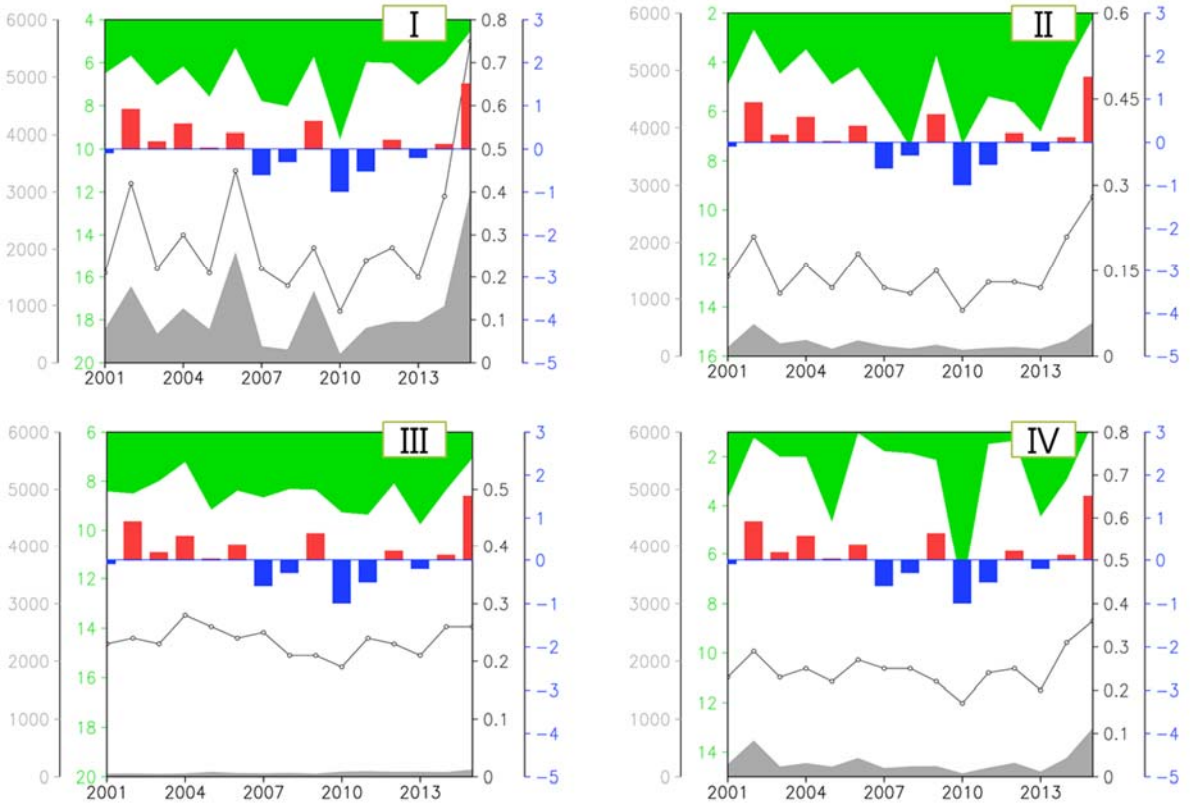

Figure III-6. Inter-annual variability (JJASO) of AOD (black line), Precipitation (green shaded), fire (grey shaded), and ENSO index (red-blue bar) during 2001-2015

The inter-annual variability of AOD, precipitation, fire, and ENSO index during 2001-2015 is plotted in Fig. III-6. The black line, green shaded, grey shaded, and red-blue bar stands for the AOD, precipitation, fire, and ENSO index, respectively. In region I, specifically, the inter-annual variability indicates that the AOD goes along with the fire positively through year to year whereas the precipitation negatively. It is also showing that most of the high AOD is usually occurring during the El-nino years such as 2006, 2009, 2015, etc. and low AOD appears during the La-nina years such as 2007, 2010, etc. Table III-2 shows that the correlation between AOD and fire is 0.96, 0.9, 0.05, and 0.85 for region I, II, III, and IV, respectively. The correlation between ENSO to AOD, fire, and precipitation is summarized in Fig. III-7.

Table III-2. Correlation of seasonal cycle of fire count, aerosol optical depth, and precipitation averaged during 2001 – 2015

	Region I			Region II			Region III			Region IV		
	AOD	FIRE	RAIN	AOD	FIRE	RAIN	AOD	FIRE	RAIN	AOD	FIRE	RAIN
AOD	-	0.96	-0.79	-	0.90	-0.84	-	0.05	-0.48	-	0.87	-0.7
FIRE	0.96	-	-0.81	0.90	-	-0.82	0.05	-	0.06	0.87	-	-0.54
RAIN	-0.79	-0.81	-	-0.84	-0.82	-	-0.48	0.06	-	-0.7	-0.54	-
ENSO	0.83	-0.82	0.85	0.84	-0.88	0.88	0.44	-0.71	0.1	0.71	-0.61	0.83

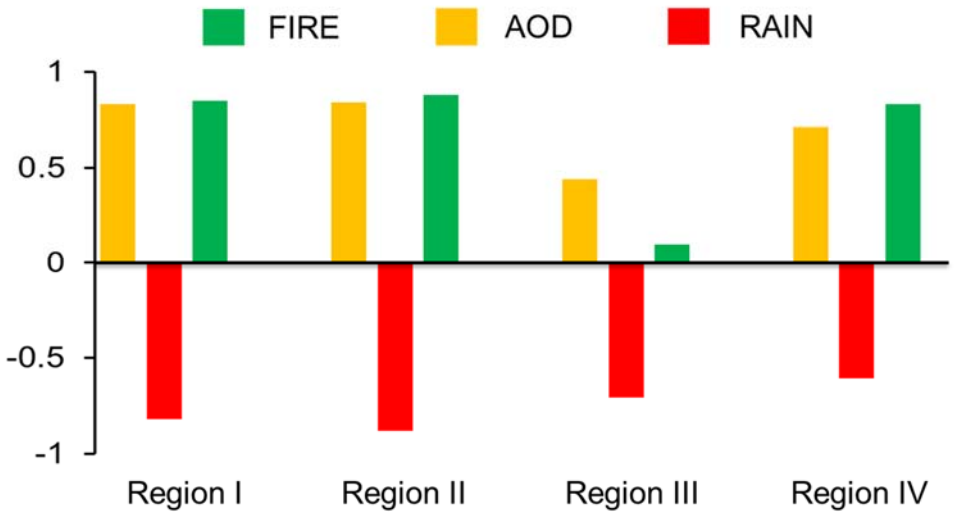

Figure III-7. Correlation between ENSO and AOD, Fire, Precipitation

The above data analysis section shows that most of the high AOD value in the main study region (region II) is contributed by the biomass burning (fire) in association with precipitation as the sink of the AOD. The AOD is further investigated to understand which AOD component is mostly contributing to the total AOD value by examining its specific detail components including organic carbon (OC), sea salt

(SS), black carbon (BC), dust (DU) and sulfate (SU). Figure III-8 indicates that during the intense biomass burning such as 2006, 2013, 2014, 2015, etc, there is high proportion of organic carbon generated, which accounts for 60 – 70 % in total quantitatively. Other components such as SU, BC, DU and SS have smaller proportions, and not much increased during the biomass burning.

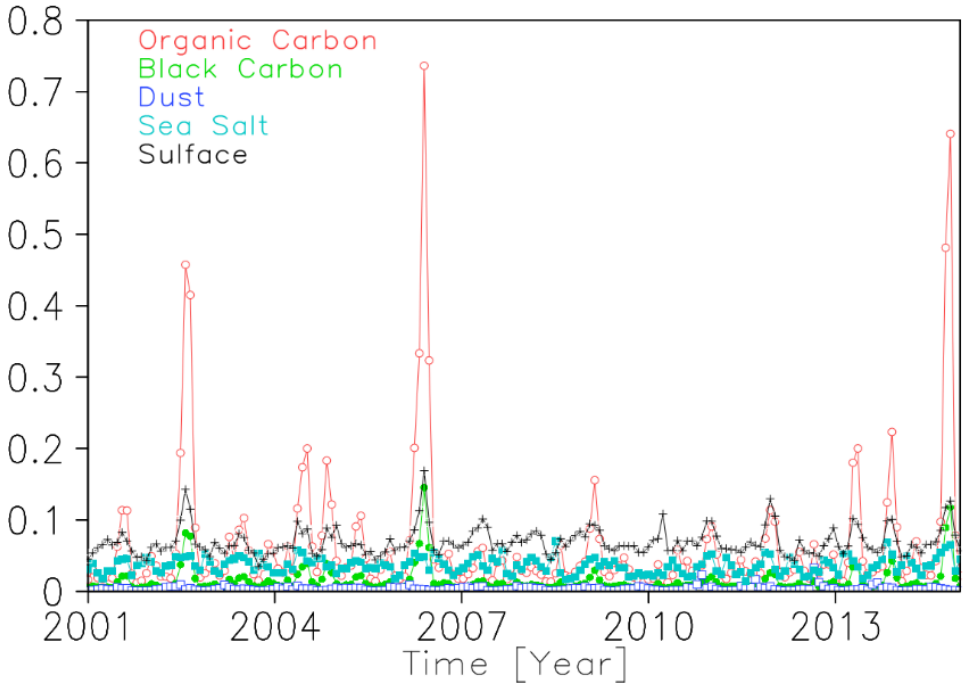

Figure III-8. Aerosol proportion in MERRA 2

In order to quantitatively estimate each AOD components in each years, the domain-averaged value of OC, BC, SU, SS, and DU is calculated as in Fig. III.9. it can be seen that large proportion of AOD is contributing by the OC, SU, and SS throughout each years. This is interesting because the sulfate is not much generate during the biomass burning as discussed above. The BC value is about 6 – 7 times smaller compared to the OC and dust amount is not much in the study regions. Calculating the correlation between each AOD components and ENSO (Fig. 10) shows that there is high correlation between OC, BC, SU, and SS to ENSO and relatively low correlation with dust. The region for its high correlation with OC and BC is due to the biomass burning which usually occurs during the El-nino years as discussed above. For the SS, it can be suggested that high sea surface temperature in Maritime continents during the El-nino years is expected to evaporate more sea salt to the atmosphere. For the SU, mostly contributed by the industrial area, it is suggested that high correlation between SU and ENSO can be due to weak wet removal mechanism or intense chemical activities during the dry period.

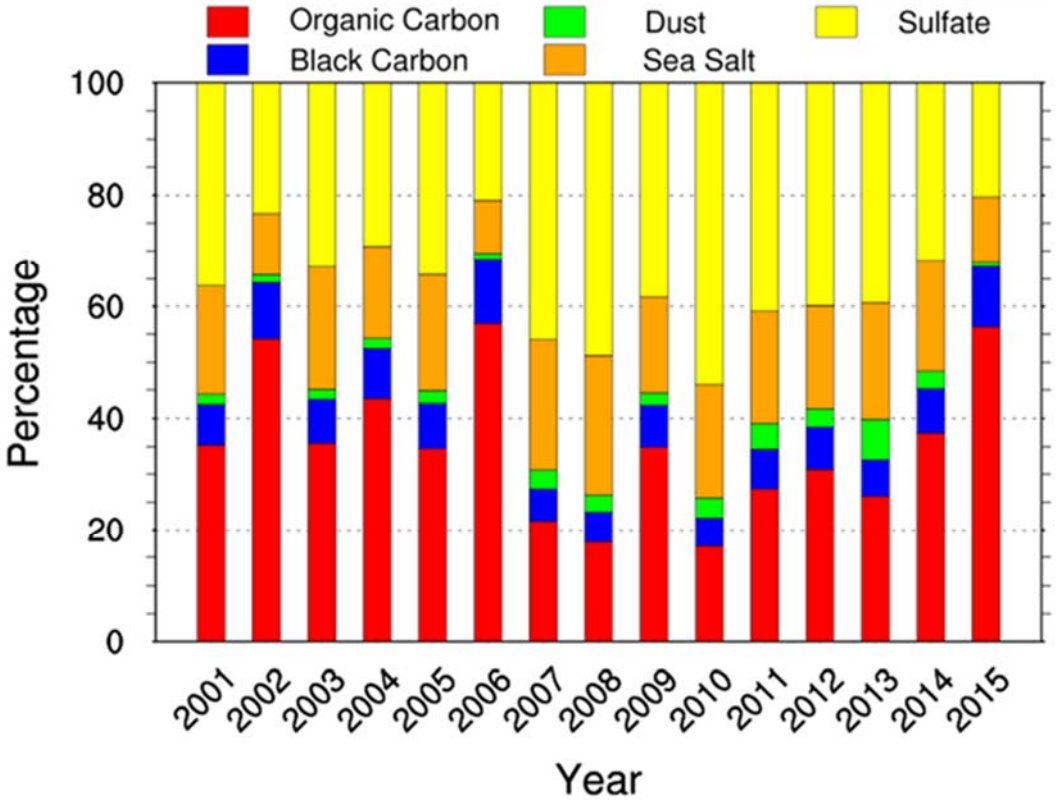

Figure III-9. AOD components retrieved from MERRA-2 model, averaged during JJASO period

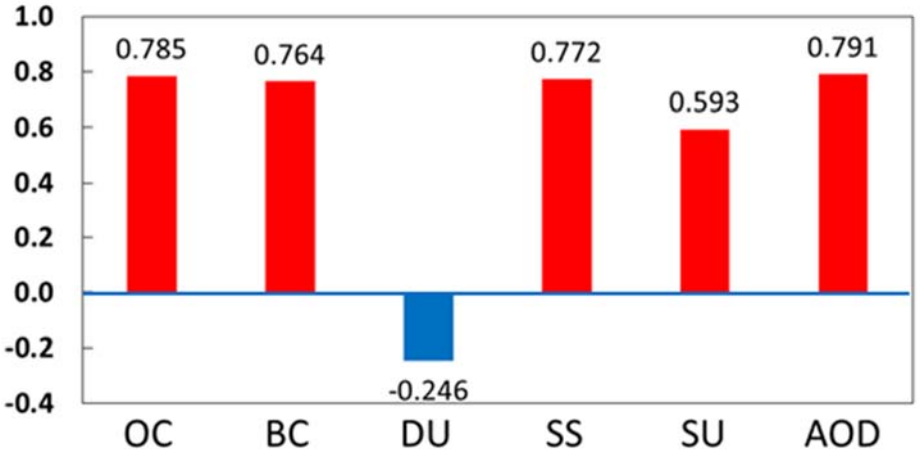

Figure III-10. Correlation between ENSO and each component during JJASO period from 2001 – 2015

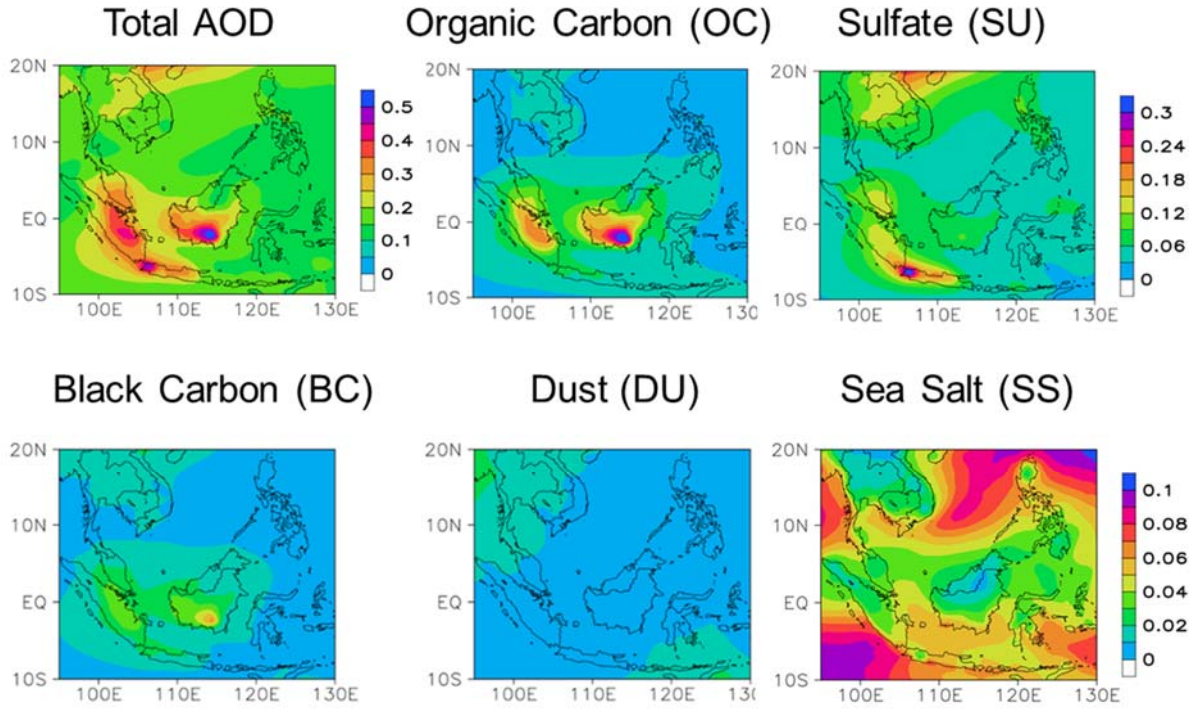

Figure III-11. Monthly aerosol components: organic carbon, black carbon, dust, sulfate, sea salt, and total AOD during 2001 – 2015

As indicated in Fig. III-10, there is a roughly equal amount of OC and SU during the JJASO period from 2001 to 2015. We further examine each contribution by plotting the spatial distribution map of OC, BC, SU, DU, and SS (Fig. III-11). The first top-left figure is the total AOD, as discussed above, it is the total of OC, BC, SU, SS, and DU. In case of OC and BC, it can be seen that most of the OC and BC is generated at the biomass burning source such Sumatra. The ratio between OC and BC is about 6 – 7 times, quantitatively. In the sulfate pattern, it can be seen that there is no specific hot spot that indicates the SU is generated from biomass burning. Mostly, it is generated from Jakarta industrial region. It is noticeable that event SU is from the industrial region, its average value still shows roughly equal amount compared to the OC during the biomass burning. For the DU, it is speculated that most of dust comes from other region to the study domain such as Myanmar, China in the north and Australia in the south. The SS also contributes to the total AOD with smaller magnitude.

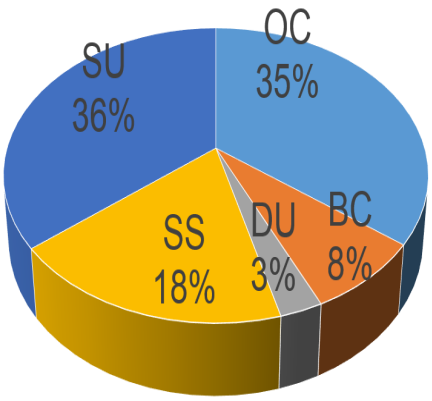

The bar graph in Fig III-12 shows the percentage of each AOD components during the JJASO period. SU amount (36%) is slightly higher than OC (35%). Both values are the most contributor to the total AOD. The following high proportion is the SS with 18%. The BC and DU accounts for 8% and 3%, respectively.

Figure III-12. Percentage of AOD components during JJASO

3.2. Evaluation of the Model Simulation

3.2.1. Winds

Fig. III-13 shows the spatial distributions of the model simulated zonal and meridional wind components (1º x 1º) at 850 hPa in comparison with MERRA reanalysis in June, 2013.

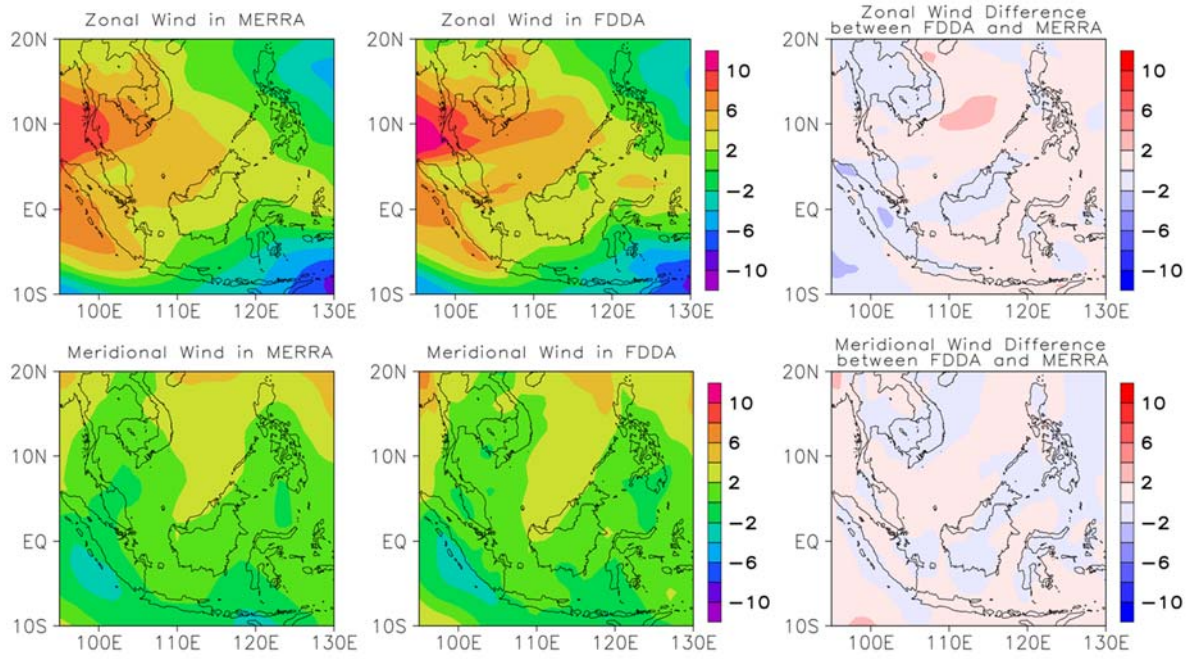

Figure III-13. Observed zonal and meridianal wind from MERRA (leftmost figures) and simulated wind for the FDDA scenarios (middle figures), and its differences (rightmost figures)

Firstly, in the case of WRF-Chem simulation with FDDA, the spatial distributions in both model and observation are relatively similar. The model simulated zonal and meridional wind components slightly

overestimates in the northern part of Maritime continent (100–120º E, 5–10º N). In contrast, it slightly underestimates the zonal wind over the Samatra and the south of Maritime continent (95–130º E, –10–10º N). There are several factors restricting the model accuracy in simulating the winds such as errors in the initial and lateral boundary conditions, large scale pressure gradient simulated in the model, or not well representation of topography due to coarser grid resolution (30 km in this case). The model simulated domain-wide average value of zonal wind is 1.12 ± 4.29 compared to MERRA value of 2.08 ± 3.58 with the mean bias of 0.96 and RMSE of 2.050. The model simulated domain-wide average value of meridional wind of 1.47 ± 1.69 have good agreement with the corresponding MERRA value of 1.08 ± 1.57 with the mean bias of -0.39 and RMSE of 1.329. Compared among the three scenarios CTR, EX1, and EX2, the model shows no significant differences.

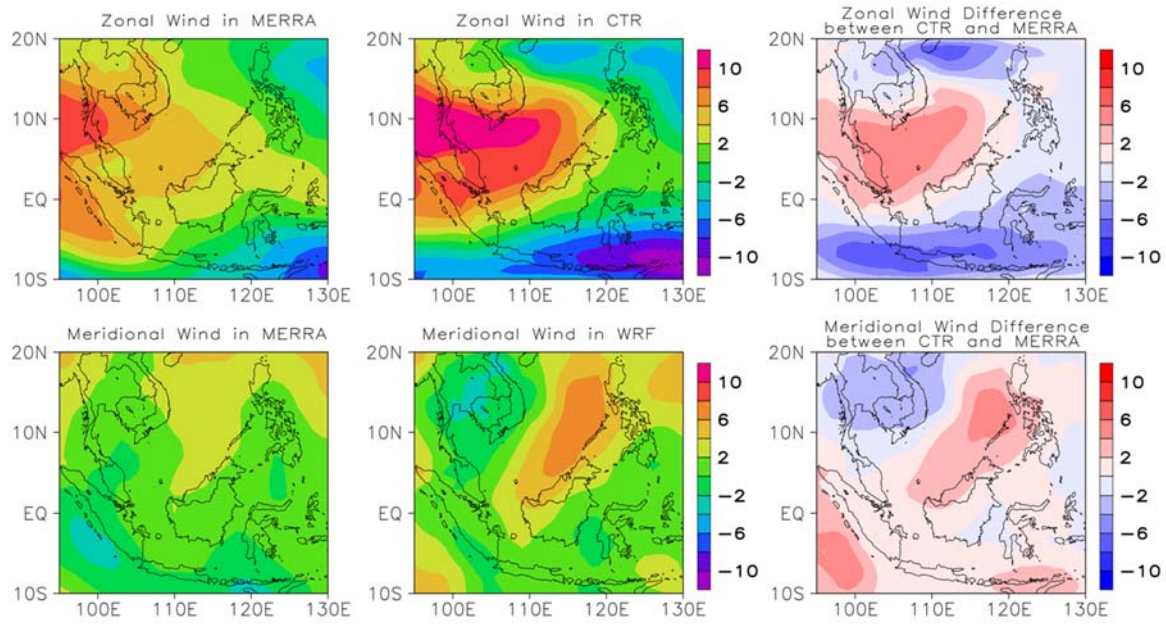

Figure III-14. Observed zonal and meridianal wind from MERRA (leftmost figures) and simulated wind for the CTR scenarios (middle figures), and its differences (rightmost figures)

In the case of WRF-Chem without FDDA (CTR) case, the model shows high positive and negative bias. For the zonal wind, CTR overestimates much of the zonal wind in the west of the domain with average wind speed of 10 m/s which is about 6 m/s in MERRA. The zonal wind difference between CTR and MERRA indicates that model overestimation zonal wind in the region of 100–120º E, 0–10º N and underestimates the zonal wind in the region of (95–130º E, -10–0º N). Due to this discrepancy in overestimating zonal wind, the AOD simulation can be reduced in model simulation. For the meridional wind, CRT shows model bias on the middle part of the domain toward the north.

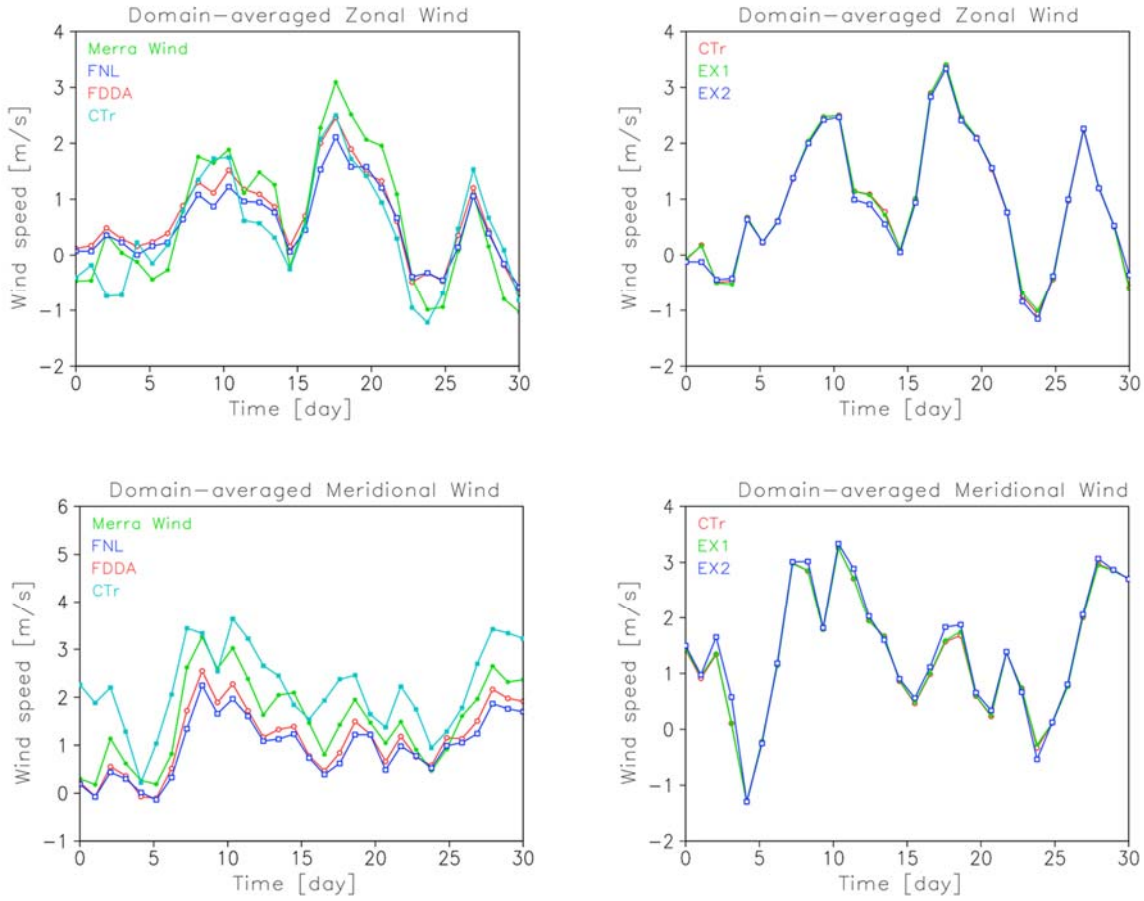

Figure III-15. The meridional and zonal domain-averaged wind in FDDA, CTR, FNL and MERRA

The domain-averaged zonal and meridional wind is showing the following figures. The two left figures are the comparison of MERRA wind, NCEP FNL wind, FDDA, and CTR case. Due to applying four-dimensional data assimilation, the zonal and meridional wind simulated in FDDA is almost similar with the NCEP FNL and comparable to MERRA data. The correlation between zonal FDDA with MERRA wind, FNL is 0.968 and 0.990, respectively. The correlation between meridional FDDA with MERRA wind, FNL is 0.968 and 0.994, respectively. For the case of CTR, domain-averaged zonal and meridional wind shows some difference due to without apply data assimilation. CTR meridional wind overestimates it compared to the MERRA and FNL. In zonal wind, it shows both lightly overestimate and underestimates the wind. The correlation between the meridional CTR wind with MERRA and FNL is about 0.833 and 0.784, respectively. The correlation between the zonal CTR wind with MERRA and FNL is about 0.903 and 0.888, respectively.

3.2.2. Precipitation

Fig. III-16 shows the spatial distributions of precipitation simulated by the model and observed by GPCP together with the difference (WRF-GPCP). The model reproduces precipitation is not well

compared to observation. Specifically, in the FDDA case, the model significantly underestimated precipitation during simulation periods with differences in an aspect of spatial distribution and magnitude. The most discrepancy between model and observation is in the northeast in which model overestimates the precipitation and in the northwest where model underestimates the precipitation.

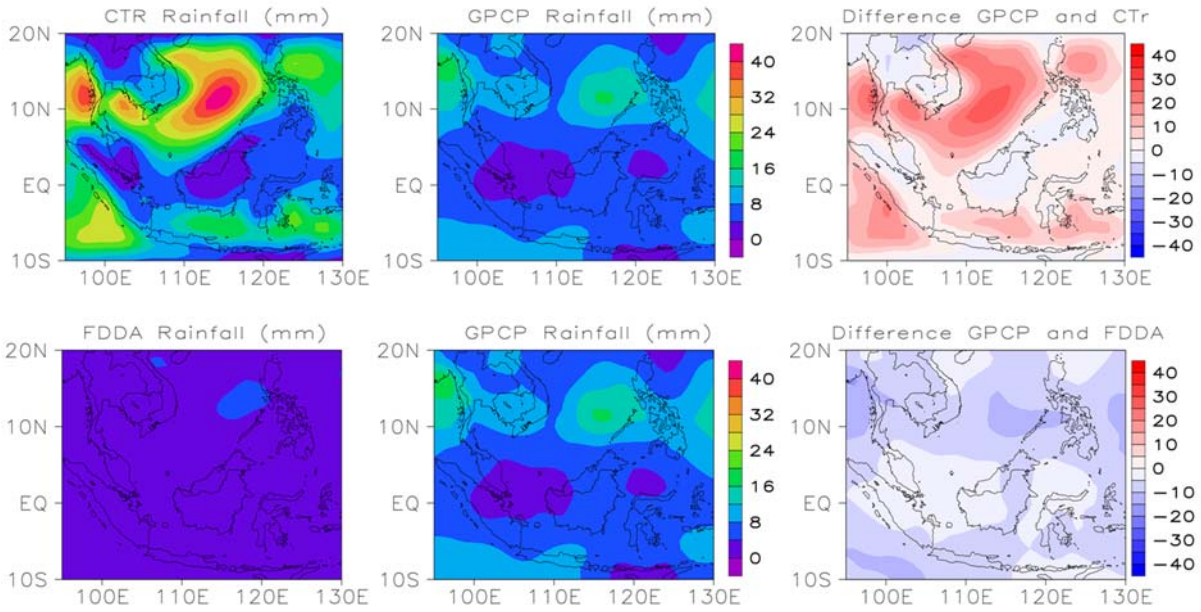

Figure III-16. Spatial distribution of co-located GPCP (leftmost figures) and WRF-Chem (middle figures) average precipitation in June, 2008. Difference (WRF- GPCP) in the average precipitation values are shown in the rightmost figures.

Overall, the difference between simulated and observed precipitation is within ± 20 mm day−1. However, the region of interest in this study is in 100–120º E,-10–10º N where the model and GPCP observation have better agreement. Due to the anomalous characteristics in tropical circulation, correct simulation of summertime precipitation over Maritime continent has been a difficult task. A number of studies reported that summer monsoonal precipitation is also not well simulated by other models such as MM5 and WRF (Rakesh et al., 2009).

3.2.3. Vertical Profiles

The following figure shows the monthly averaged vertical profiles of simulated meteorological variables compared with the MERRA reanalysis data. In general, the model vertical meteorological variables found to be in a good agreement with observation. The model reproduces well with small bias. The model overestimates the relative humidity in the lower and upper atmosphere, and underestimates it in the middle atmosphere. Wind speeds are overestimated near-surface while it is comparable in the upper atmosphere.

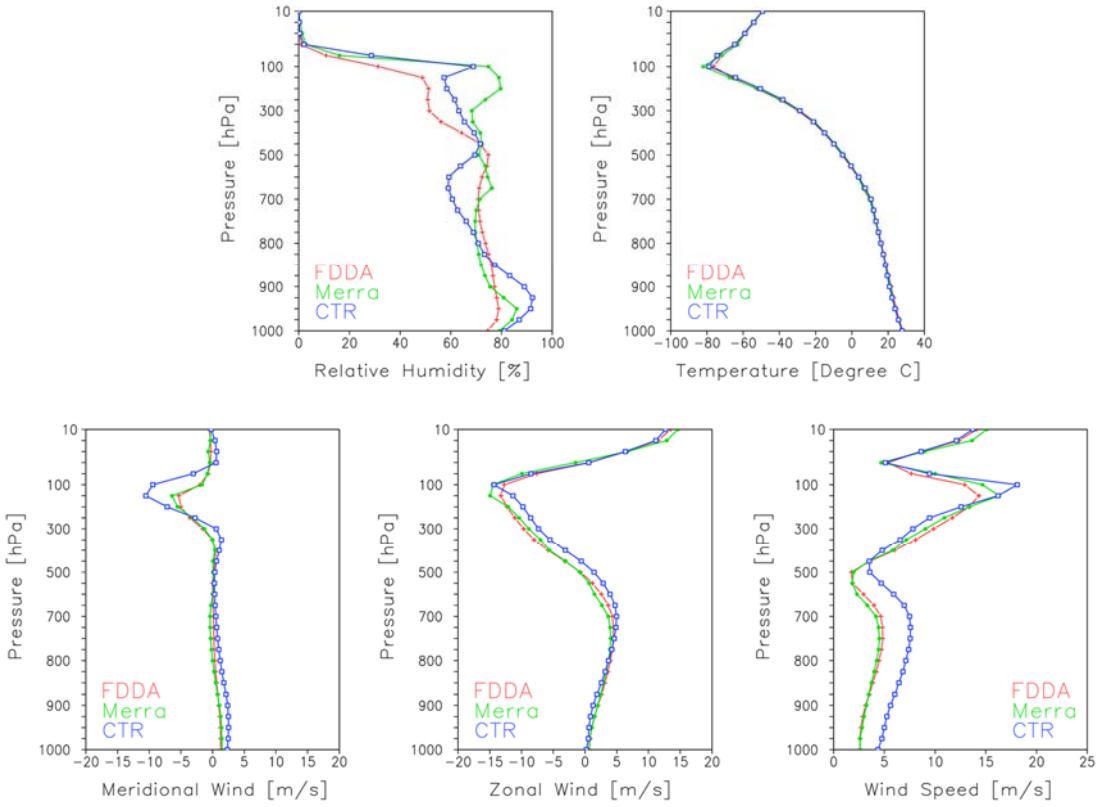

Figure III-17. The vertical profile of relative humidity, temperature, zonal wind, meridional wind, and wind speed

3.2.4. Aerosol Optical Depth

As mentioned in the section 2.2.4, the simulation time is in June 2013 and September 2015. Fig. III-18 shows the domain-averaged AOD time series in MO111DIS, CTR, and No-Fire. The correlation between MODIS and CTR is 0.84 and 0.42 for the case 2013 and 2015, respectively. On the other hand the correlation between MODIS and No-Fire simulation is 0.21 and 0.38, respectively. In 2013, the model has good correlation with MODIS compared to the No-Fire simulation when the fire emission inventory is excluded. However, in case of 2015, the model has relatively low correlation with MODIS data. There are two possible reason that are the uncertainty in MODIS satellite data and the model's capacity in capture the AOD during extremely high aerosol load as the case in 2015. Overall, the model simulation without the fire inventory indicates that it is necessary to integrate the fire emission while simulating the AOD in Southeast Asia biomass burning. So as to clearly see the difference between CTR and No-Fire simulation, Fig. III-19 shows the spatial distribution map of AOD, it is apparent that there is no signal of biomass burning in the region while fire emission inventory is not included.

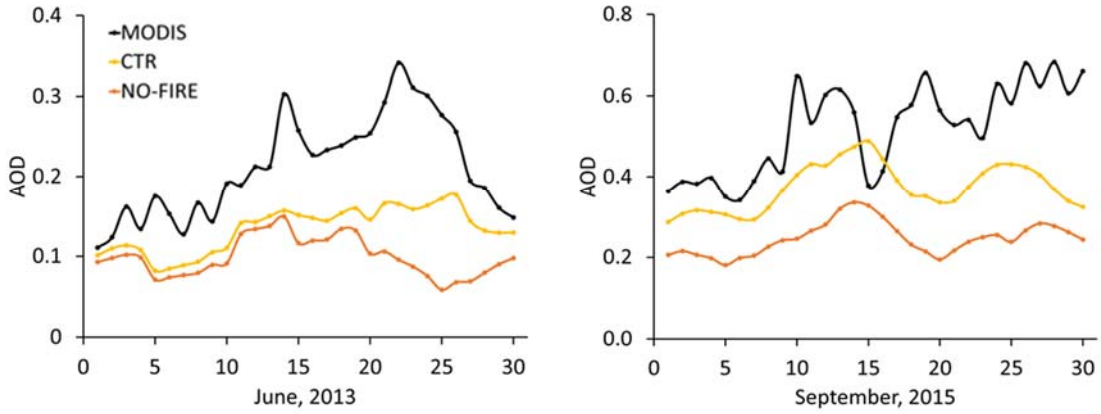

Figure III-18. Domain-averaged AOD in MODIS, CTR, and No-Fire simulations for June 2013 (left) and September 2015 (right case)

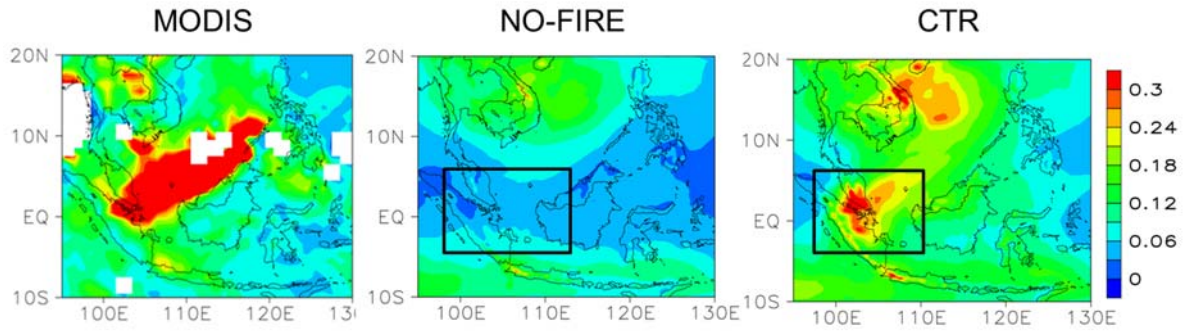

Figure III-19. Spatial distribution of AOD in MODIS (left), No-Fire (middle) and CTR (right) in June 2013. Black box indicates the fire emission source in No-Fire and CTR

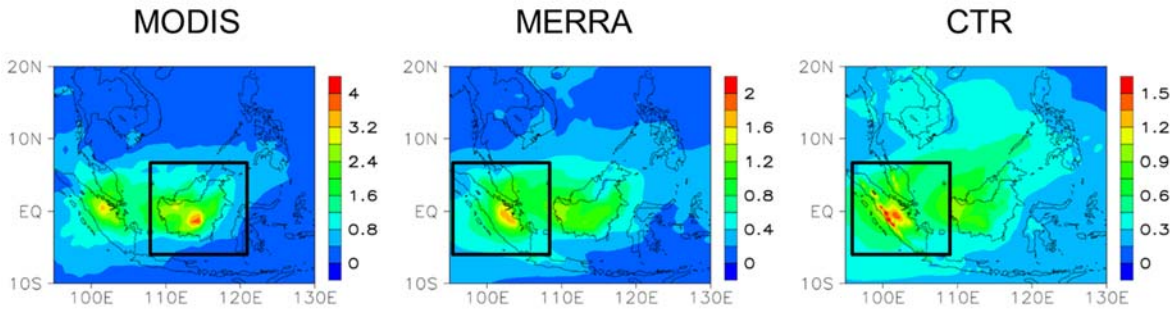

Figure III-20. Spatial distribution of AOD in MODIS, MERRA, and CTR in September, 2015. The black box indicates the original fire emission source

The above explanation emphasizes the importance of including the fire inventory in model simulation. Fig. III-20.shows the spatial distribution of AOD during the biomass burning in September, 2015 case. The AOD pattern is plotted at different scale for the reason of pointing out the main fire source in MODIS, MERRA, and CTR. As in MODIS case, the black box indicates it that the main source of fire

is in the Kalimantan region. However, it is in the Sumatra region. In the MERRA-2 case, the AOD is driven by GOCART. It can be suggested that both MERRA and WRF-Chem CTR simulation have bias in fire emission inventory which in turns leads to underestimate AOD concentration in the simulation compared to MODIS. In this section, the AOD value in WRF-Chem CTR will be compared with the FDDA cases. As mentioned earlier, in the FDDA case, the meteorological variable such as horizontal winds, moisture and temperature are nudged with a nudging coefficient of 6×10^{-4} s^{-1} at all vertical levels. This in turn helps model reproduce relatively high wind speed, temperature, etc compared to the CTR case. Fig. III-21 shows the spatial distribution of AOD MODIS, MERRA, CTR, and FDDA from the left to the right for June 2013 case. The lower panel is plotted at smaller scales. In the case of CTR, it is overestimated AOD in the northern site of the domain (e.g. cities) and underestimated AOD in the main fire regions. However, in case of FDDA, model reproduced abnormal AOD pattern in the northeast site of the domain, which is mainly at sea and have no specific source of aerosol contribution. FDDA is further examined by checking the correlation between FDDA to MODIS and MERRA. The correlation is 0.33 and 0.31 for MODIS and MERRA, respectively. This is relatively low compared to the CTR simulation.

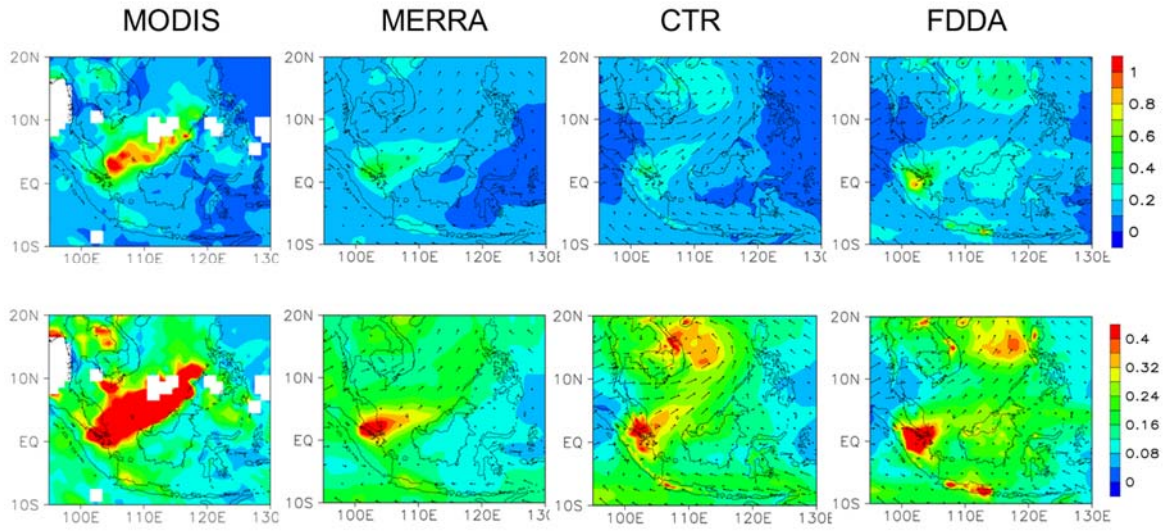

Figure III-21. Spatial distribution of AOD in MODIS, MERRA, CTR, and FDDA (left to right) for June 2013. Lower panel is plotted with smaller scale

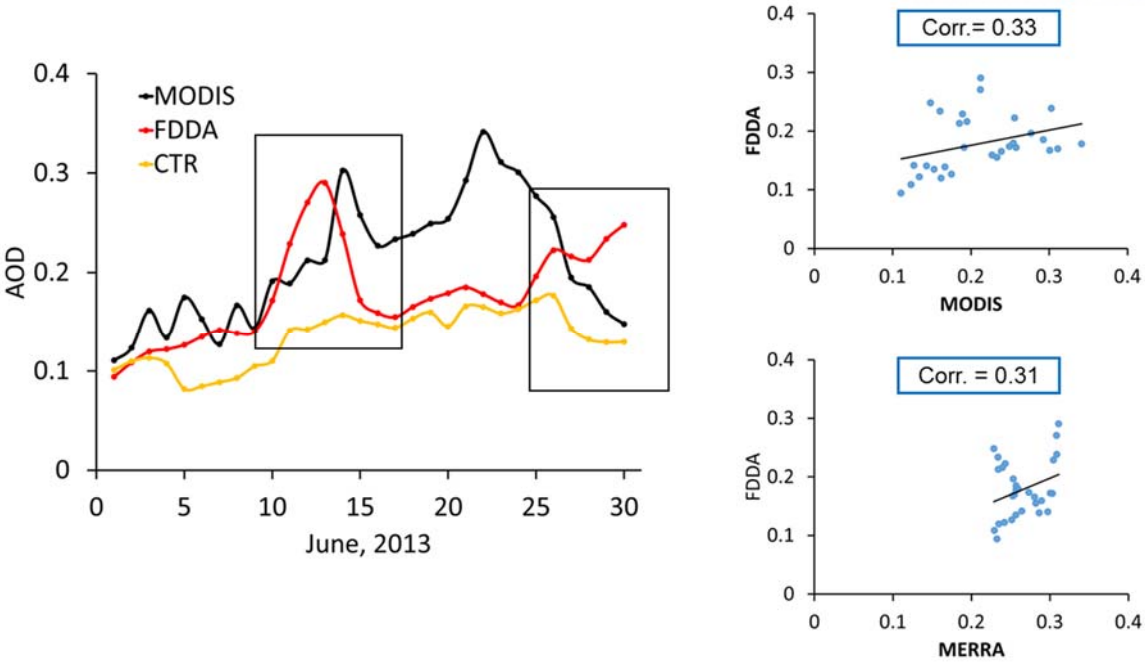

Figure III-22. Domain-averaged of AOD in MODIS (black-line), FDDA (red-line), CTR (yellow-line) on the left and the scatter plot of FDDA to MODIS and MERRA on the right during June 2013

The temporal evolution time-series at six sites of WRF-Chem simulated AOD at 500 nm are compared with co-located AERONET observations during 01 – 30 June 2013 (below figure). The first thing to notice in this figure is that there is no completely continuous time series of AOD measured by AERONET during the simulation period. For the AERONET station data, the available temporal series AOD data is not always continuous (e.g. hours, days, weeks) even though it is set to monitor and measure every 15 minutes. In addition to the main reason that cloud interference leads to reduce data availability, the other reasons can be instruments temporarily off for maintenance, etc. Under those circumstances, the hourly AOD data are not available and incomplete. The dark blue, red, green, purple, light blue and orange stand for CTR, EX1, EX2, FDDA, AERONET, and MODIS, respectively. In June, 2013, the biomass burning first started in the Sumatra region. The most nearby AERONET station to the source region is Singapore and Jambi. Pontianak and Kuching as the two AERONET station downwind, and the other two are located far from the biomass source.

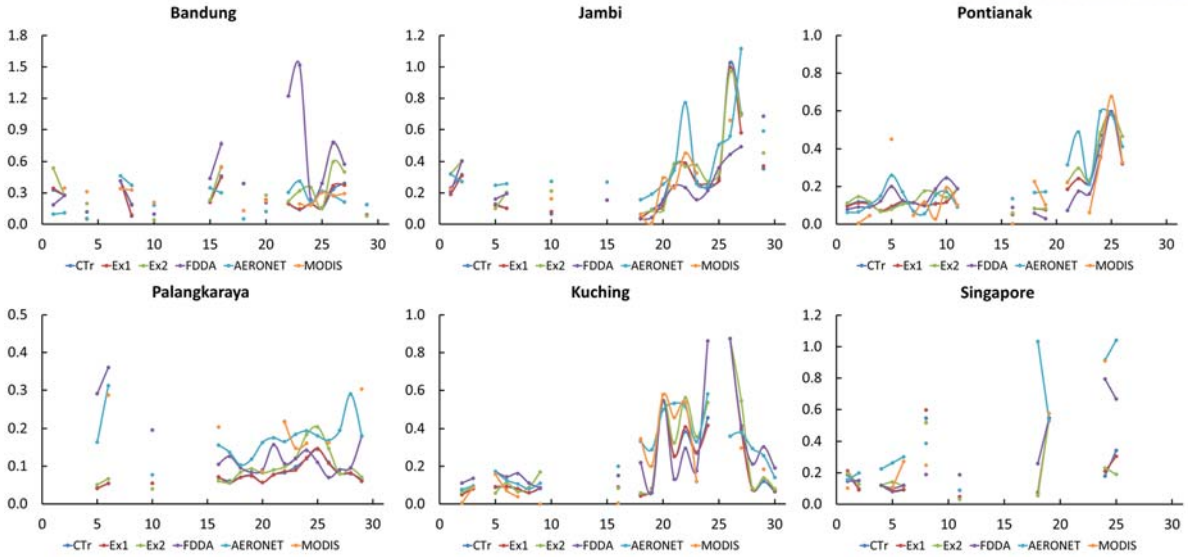

Figure III-23. Variations in co-located AERONET observed and WRFChem simulated aerosol optical depth at 550 nm at six sites located in the model domain during 01–30 June 2013. The dark blue, red, green, purple, light blue and orange stands for CTR, EX1, EX2, FDDA, AERONET and MODIS

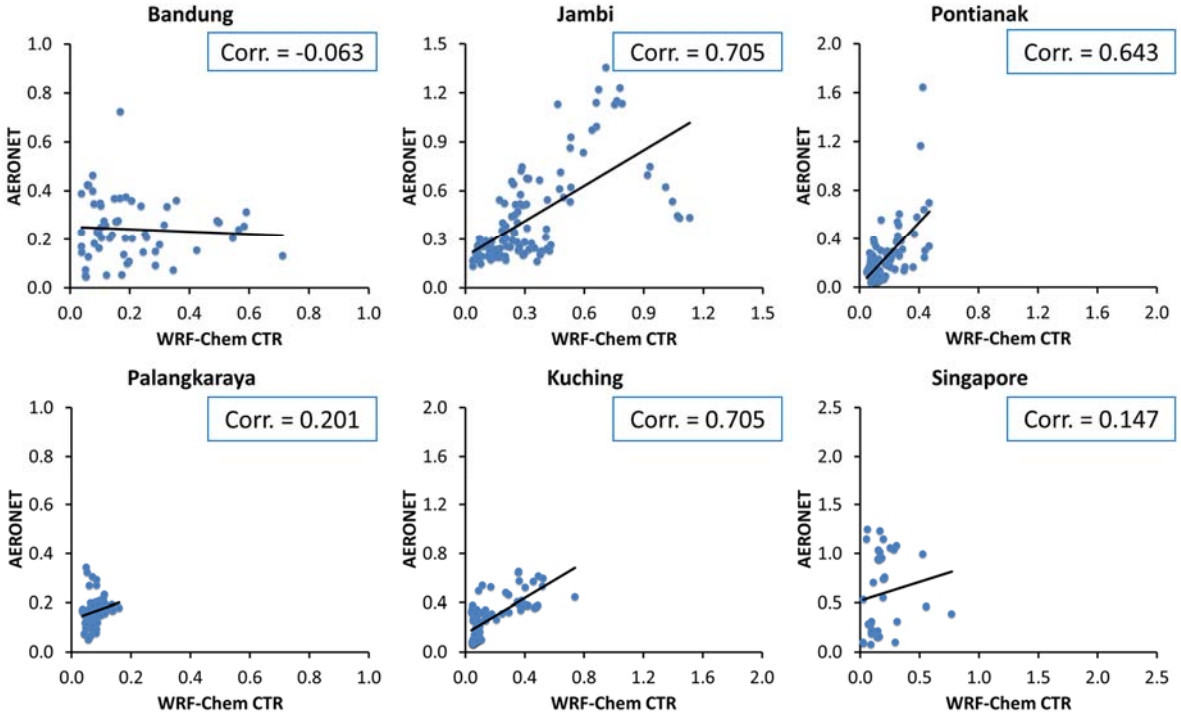

Figure III-24. Scatter plots of hourly mean AOD between AERONET and WRF-Chem in June 2013

At Singapore, comparison between model and AERONET shows that the model was able to capture the first few day from 01 – 10 June, however, it fails to represent AOD and overestimate it during the high intense biomass burning on 24 – 25 of June, with the AOD of almost double compared to AERONET station. The correlation between the Singapore station and CTR is 0.147. Similar tendency is also

expected in the downwind Kuching AERONET station, model seems to represent well the AOD simulation in the early of the month, but it is still showing highly overestimate AOD values during the peak of biomass burning. The correlation of this station to the model simulation is 0.705. In case of Pontianak station, it shows best comparison between AERONET station and model simulation, it can be able to capture the fluctuation in the early month as well as the peak on 24 – 25 of June. Although there is no aerosol data assimilation being applied in this study, but this correspondence indicates model ability in simulation AOD at single point location. The hourly correlation with AERONET station is only 0.643. The two other station Bandung and Palangkaraya also displays a similar trend in overestimate the AOD value. In Bandung, the model seems to be unable to capture the biomass burning signal due to it is located in the metropolitan area with high diurnal AOD cycle. Overall, model shows high possibility of overestimate AOD during the biomass burning event at single point location.

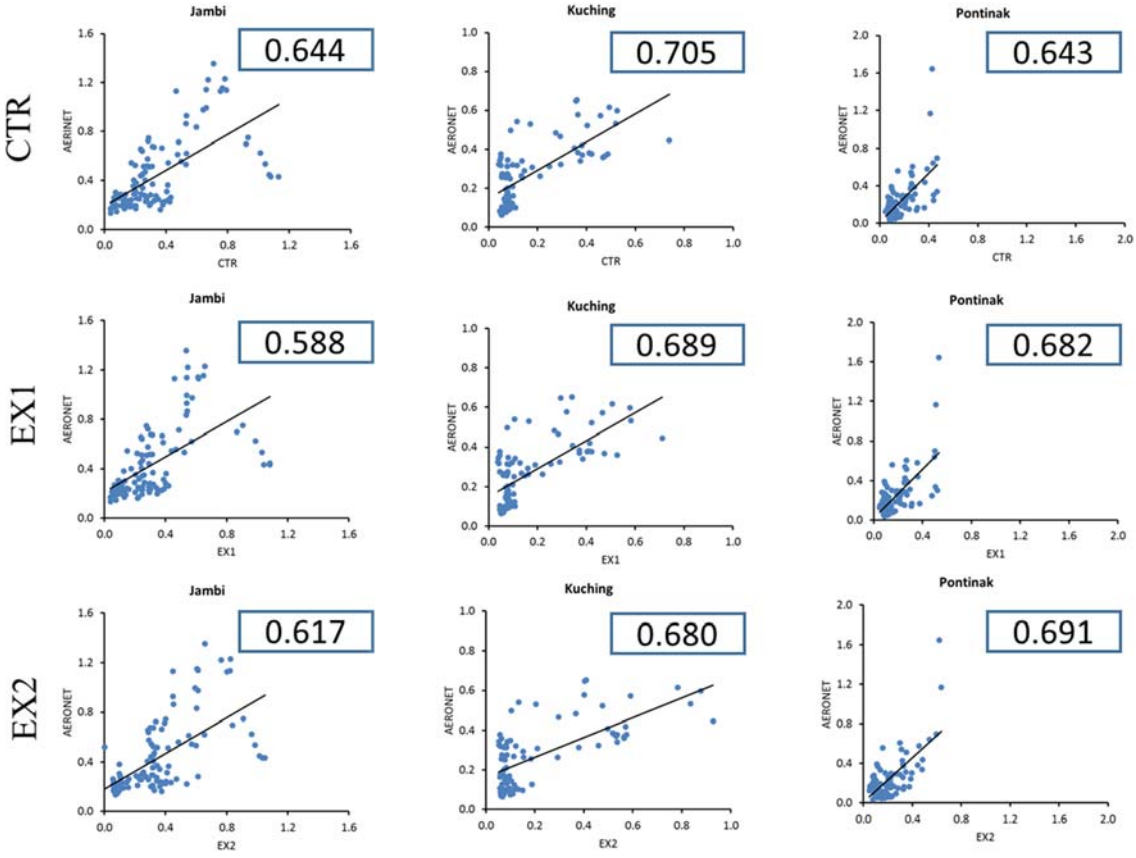

Figure III-25. Scatter plots of hourly mean AOD between AERONET and 3 scenarios

Fig. III-25 shows the scatter plot of hourly mean AOD between AERONET and 3 scenarios. In general, there is not much difference in model simulation of AOD at single grid point in all 3 CTR, EX1, and EX2 cases. The correlation is roughly equal among 3 cases.

3.3. Aerosol Impacts on Meteorology and Air Quality

3.3.1. Impacts on Meteorological Fields

The temporal and spatial distribution of aerosol is highly influenced by meteorological variables including air temperature, solar radiation, and wind speed. The inclusion of both aerosol direct and indirect effects was found to have influence on those variables. Fig. III-26 illustrates the monthly mean impact of aerosols on the shortwave radiation flux (top figure), 2 m temperature (middle figure), and the PBL height (bottom figure) over Maritime continent in September 2015. The monthly mean value, direct effect (EX1 – CTR), indirect effect (EX2 – EX1) and total effect (EX2 – CTR) as from the left to the right of Fig. III-26. The shortwave radiation flux at the ground is highly influenced by both aerosol direct and indirect effect. In the aerosol direct effect case, more downward shortwave radiation flux is reduced in the main biomass burning region, whereas it is mostly in the southern sea in the aerosol indirect effect. In the aerosol indirect case, the land-ocean signal of reducing downward shortwave radiation is not clear since the shortwave radiation reduction in land does not change much.

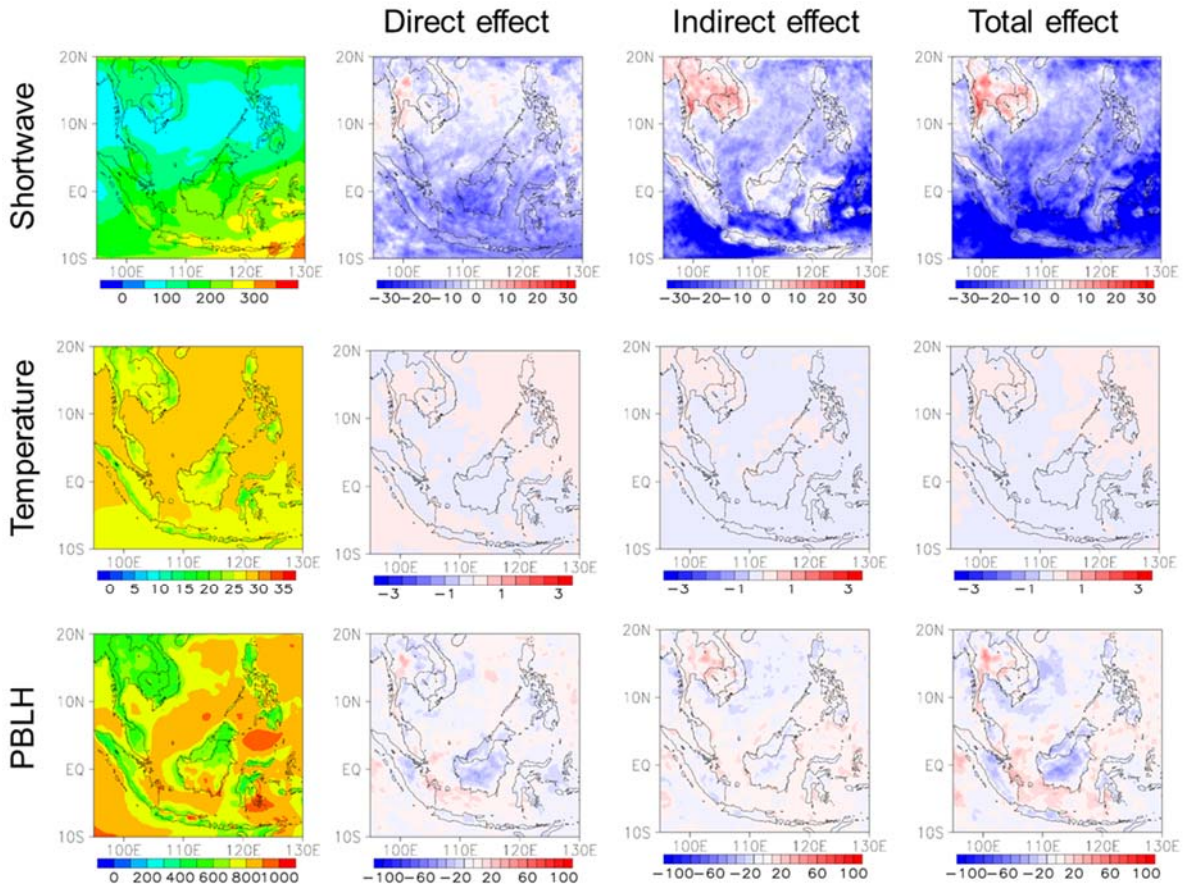

Figure III-26. Simulated total effects (EX2 − CTR), direct effects (EX1 − CTR) and indirect effect (EX2 – EX1) on shortwave radiation flux at ground, 2 m temperature, and the PBL height in September 2015.

Aerosols intercept shortwave radiation reaching the surface in several ways. First, particles directly scatter (first aerosol direct effect) and absorb (second aerosol direct effect) incoming solar radiation, resulting in surface dimming. Secondly, in-cloud particles change cloud lifetime and albedo, thus, causing variations of shortwave radiation at the ground surface. As shown in Fig. III-26, the downward shortwave radiation flux at the ground is reduced over the Maritime continent by up to −65.0 W m^{-2} in the aerosol radiative effect and 94.0 W m^{-2} in the aerosol indirect effect. This results is different with the finding in other studies such as Zang et al., 2015 found that downward shortwave radiation flux mainly results from the aerosol radiative effects in China regions and Forkel et al., 2012 stated that it is mainly resulted from the aerosol indirect effect in Euro regions. In general, when the near-surface shortwave radiation flux is decreased due to the aerosol effect, near-surface energy fluxes are suppressed which leads to weaker convection and mainly longwave radiation is emitted to the near surface. Decreasing the shortwave radiation results in surface cooling which in turn reduces 2 m temperature, and the PBL height is also reduced by up to 95 m. In case of 2m temperature, it is decreased in both aerosol cases but only with small amount (less than 10% of the monthly mean 2 temperature). The PBL height is expected to reduce due to the reduction in the shortwave radiation and 2 temperature. Its signal is clearly shown in the aerosol direct case that the PBL height is decreasing, but it is unclear signal in the indirect case due to smaller reduction compared to the direct case. Meteorological variables such as wind speed, air temperature, and the PBL height can also be affected by land surface properties. The aerosol direct and indirect effects during the biomass burning are both found to alter solar radiation, temperature or the PBL height over Maritime continent. In general, the near-surface atmosphere is more stable when aerosol feedback is included in simulation, which enhances near-surface pollution accumulation.

The model overestimates precipitation for most regions in Maritime continent compared to the GPCP data. Comparison among three aerosol simulations shows that aerosol indirect effect produces more precipitation than the base and direct effect simulation. Cloud and precipitation formation mostly develops in the north of study domain (Indochina) and over the ocean (as shown in Fig. III-27 and Fig. III-28). Aerosol indirect effects can change cloud properties such as cloud lifetime, and precipitation rate and effective radius directly. As shown in Fig. III 28, aerosol direct effect plays small role in changing cloud properties whereas aerosol indirect effect is more significant, mainly in the north. Cloud water path is also decreased over in the aerosol indirect effect. In other studies such as Forkel et al., 2012 indicated that the aerosol indirect effect is more important in altering solar radiation, temperature, and the PBL height. However, in other studies such as Zhang et al., 2013 found that aerosol direct effects is more important on the near-surface shortwave radiation flux, 2m temperature, wind speed at 10 m, and the PBL height. Different from these studies, our study finds that both aerosol indirect and direct have influence on meteorological variables.

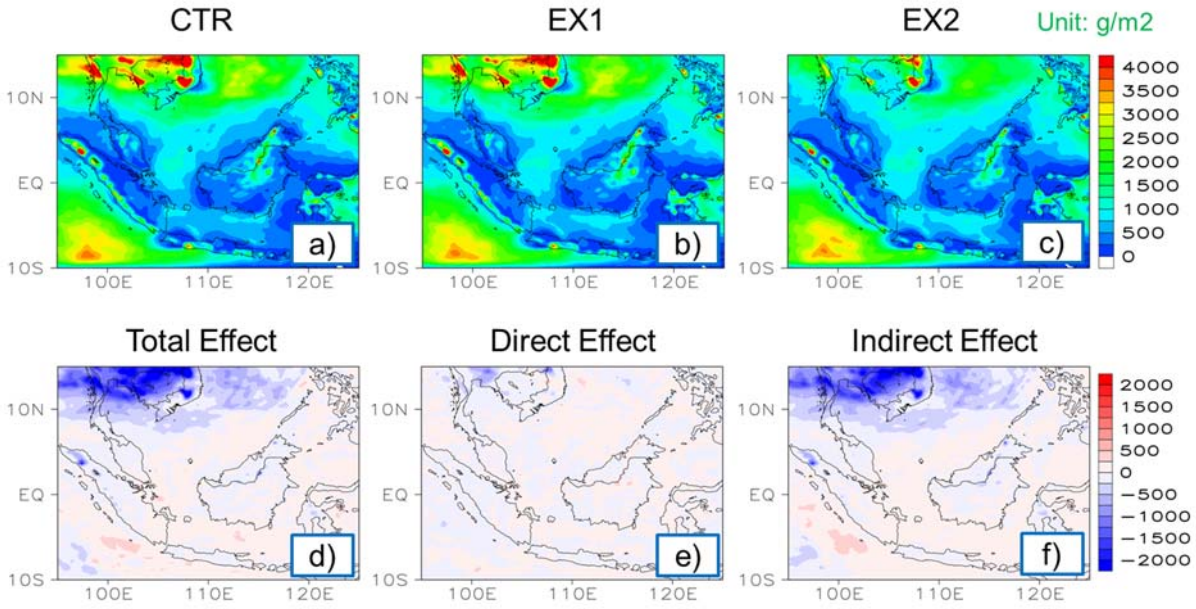

Figure III-27. Monthly simulated cloud water path (a-c) for 3 scenarios and aerosol total effect (EX2 − CTR) (d), direct effect (EX1 − CTR) (e) and indirect effect (EX2 − EX1) (f)

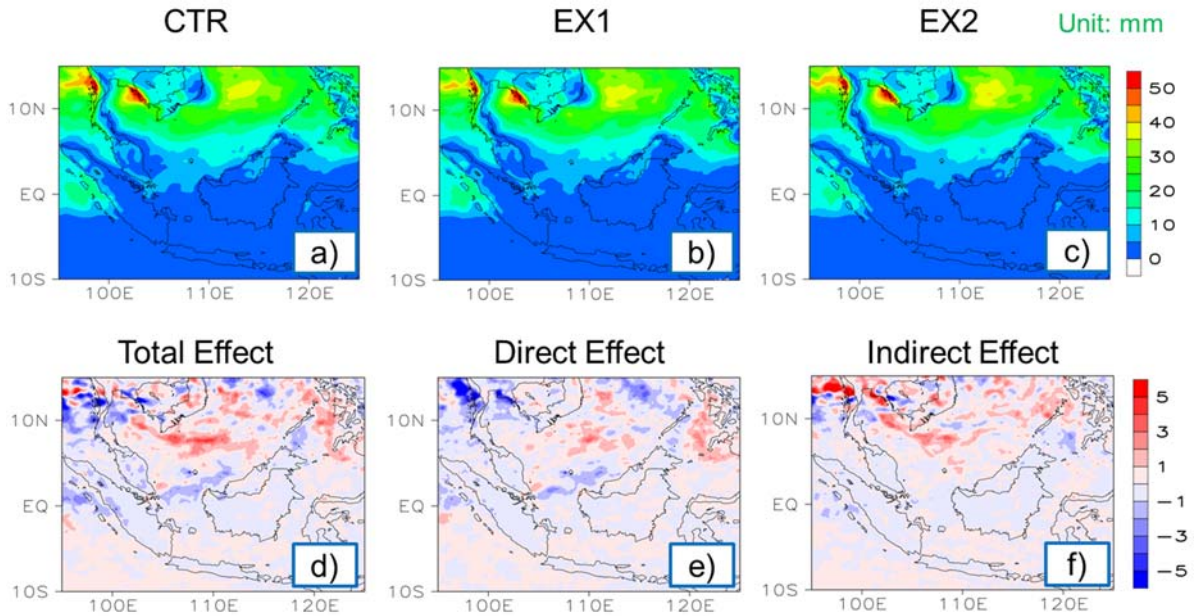

Figure III-28. Monthly simulated precipitation (a-c) for 3 scenarios and aerosol total effect (EX2 − CTR) (d), direct effect (EX1 − CTR) (e) and indirect effect (EX2 − EX1) (f)

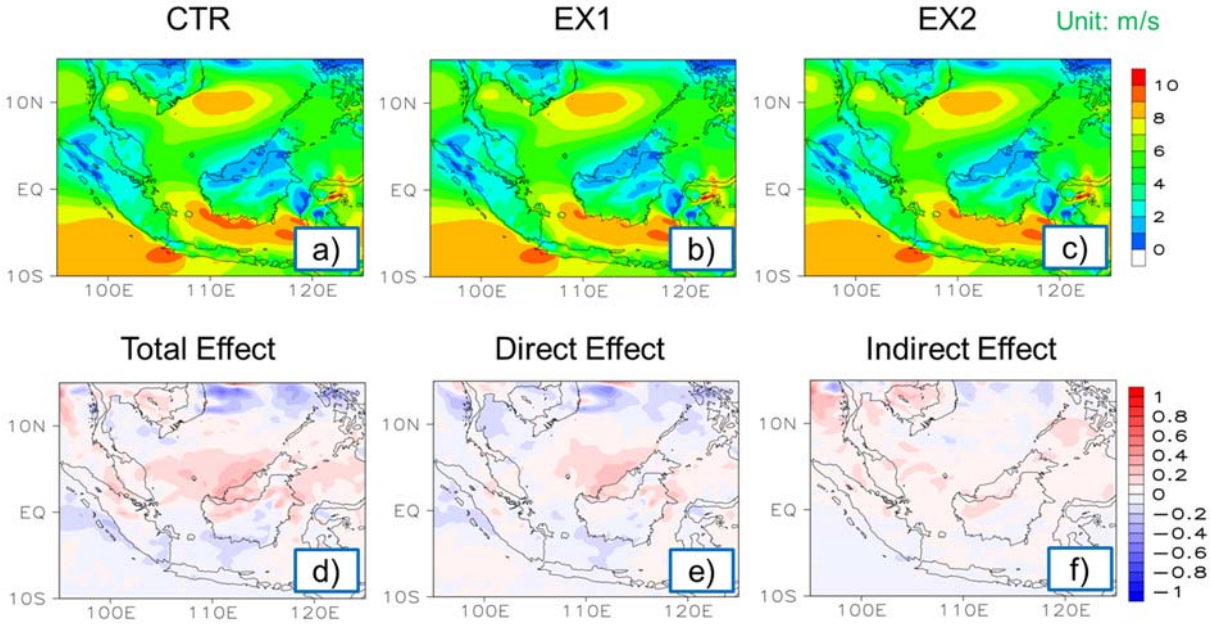

Figure III-29. Monthly simulated wind (a-c) for 3 scenarios and aerosol total effect (EX2 − CTR) (d), direct effect (EX1 − CTR) (e) and indirect effect (EX2 − EX1) (f)

3.3.2. Impacts on Air Quality

The aerosol effects not only can moderate meteorological variables, but also greatly impacts on air quality. Fig. III-32 shows spatial distributions of SO_2, NO_x, CO, and O_3 and the feedbacks of aerosols on these three atmospheric trace gases in September 2015. The aerosol direct effect (EX1 – CTR) and indirect effect (EX2 – EX1) is shown in the middle and the rightmost of Fig. III-32, respectively. In case of SO_2, there is almost no difference between the direct and no aerosol feedback case. The reason can be due to low aerosol loading in the region. In CTR, most of SO_2 is contributed by the big cities in the north or the industrial area such as Jakarta in the south. As discussed in the section 3.1, not much SO_2 is generated during the biomass burning, therefore, less aerosol interaction with radiation which led to almost unchanged SO_2 concentration in the two simulation. In the indirect case, the SO_2 concentration is smaller in the aerosol indirect effect than in the direct effect. This means that there is less aerosol in case of considering aerosol indirect effect which suggested that a number of SO_2 aerosol have turn from interstitial air-born aerosol to become cloud-born aerosol. For the NO_x, it is a short-live species of about 0.5 – 2 days. Therefore, most of NO_x is concentrated in the nearby emission source. NO_x is mostly influenced by the aerosol effect in which enhances more NO_x in the region. The near-surface CO concentrations are also increased when aerosol direct feedback is included. Large increases of CO are concentrated at source where biomass burning takes place with high aerosol loading. The main reason leading to increase of CO concentration may mainly result from a more stable near-surface atmosphere and a lower PBL height due to aerosol direct effects.

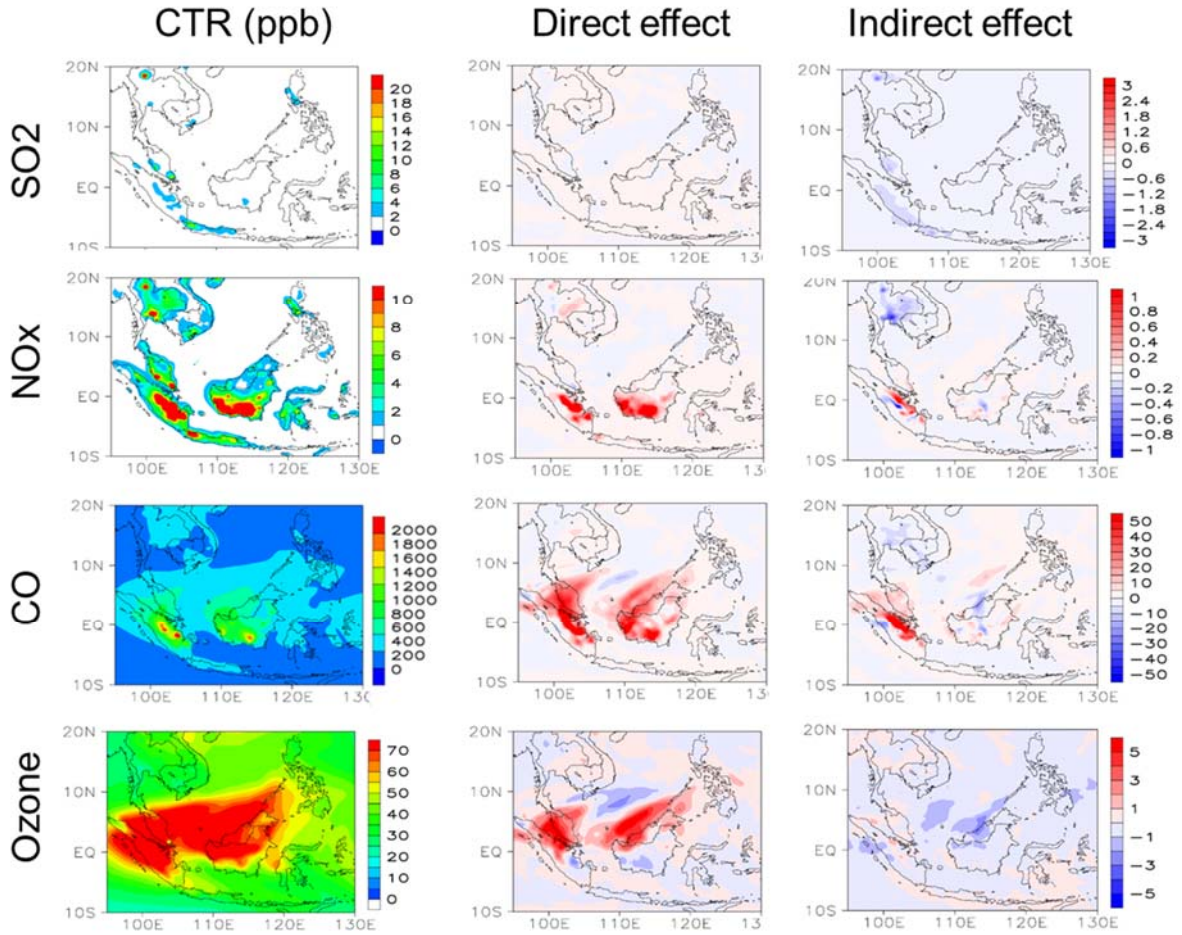

Figure III-30. Simulated monthly mean CO, SO_2, and O_3 mixing ratios and aerosol feedbacks (BASE − EMP) on the three gas pollutants over Maritime continent in September 2015

In this study, we found that the aerosol indirect does not influence the gas species much when considering aerosol feedback. The formation of O_3 is mainly due to two reasons: directly related to temperature and solar radiation in areas with sufficient NOx and VOCs which in turn increases photolysis rate; and the other region can be due to more isoprene aerosol generated. In general, due to the aerosol radiative effects, the lower atmospheric temperature and reduced incoming solar radiation lead to a decreased photolysis rate of NO_2 and accordingly reduce O_3 concentrations. However, in our study, the result is different with that idea in which O_3 concentration is only reduced at the biomass burning regions and increases in the downwind region. The reason can be for this inconsistent results compared to other studies due to the different emission in each study. Specifically, biomass burning is expected to generate more biogenic emission which has more aerosol production. When aerosol direct effect turns on, there will be more interaction between the aerosol and radiation. Although, the aerosol direct effect is expected to decrease the shortwave radiation resulting in reduce temperature led to reduce photolysis rate of NO_x, this is not the way that leads to decrease O_3 concentration because there

are large amount of NO_x producing during the biomass burning process which is a good condition for increase O_3 concentration.

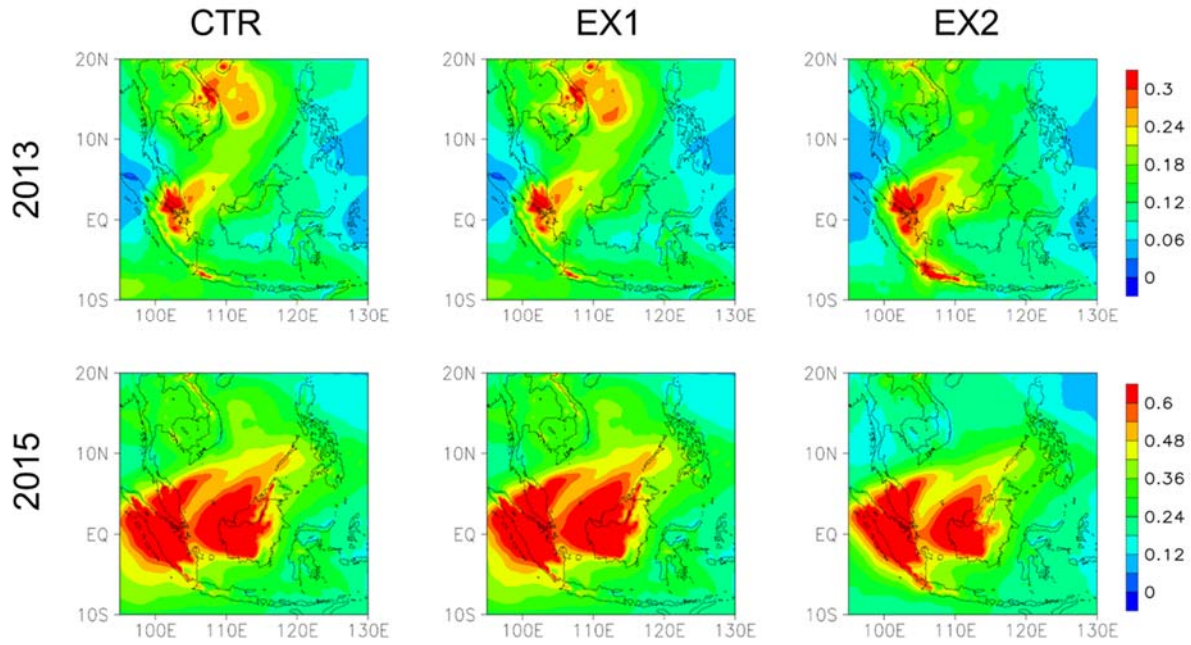

Figure III-31. Monthly mean spatial distribution of AOD simulated in 2013 (top) and 2015 (bottom) in three simulations: CTR (no aerosol effect), EX1 (direct effect), EX2 (aerosol indirect effect)

Fig. III-31 shows the monthly mean spatial distribution of AOD simulated in 2013 and 2015 in three different simulations. In case of 2013 which has lower aerosol loading compared to 2015, the distribution of AOD is almost similar in CTR and EX1, there is a smaller different in the EX2 which can be due to the change in aerosol when it interacts with cloud. The similar results are seen in case of 2015, however, with larger aerosol loading amount, the EX2 is smaller different compared to the CTR and EX1 in the 2015 case. The aerosol impacts on aerosol mass concentrations are shown in Fig. III-32. Both enhancement and reduction of AOD, $PM_{2.5}$ is found in the study domain. The aerosol impacts are further separated into direct effects and indirect effects so as to investigate the mechanisms of how AOD and $PM_{2.5}$ responds to aerosol impacts. Near-surface $PM_{2.5}$ can be impacted by the changes in many different atmospheric processes and mechanism due to the aerosol direct effects. The sulfate production, one of the contributor to the total AOD and mass concentration, can be suppressed in lower temperature condition, and the oxidation of precursors of secondary aerosols can also reduce when the solar radiation is decreasing. However, the stabilized lower atmosphere and the PBL height reduction can be the mainly significant contributors to enhance of $PM_{2.5}$ concentration caused by the aerosol direct effect, because the atmospheric primary trace gases also increase when aerosol direct effect is taken into account.

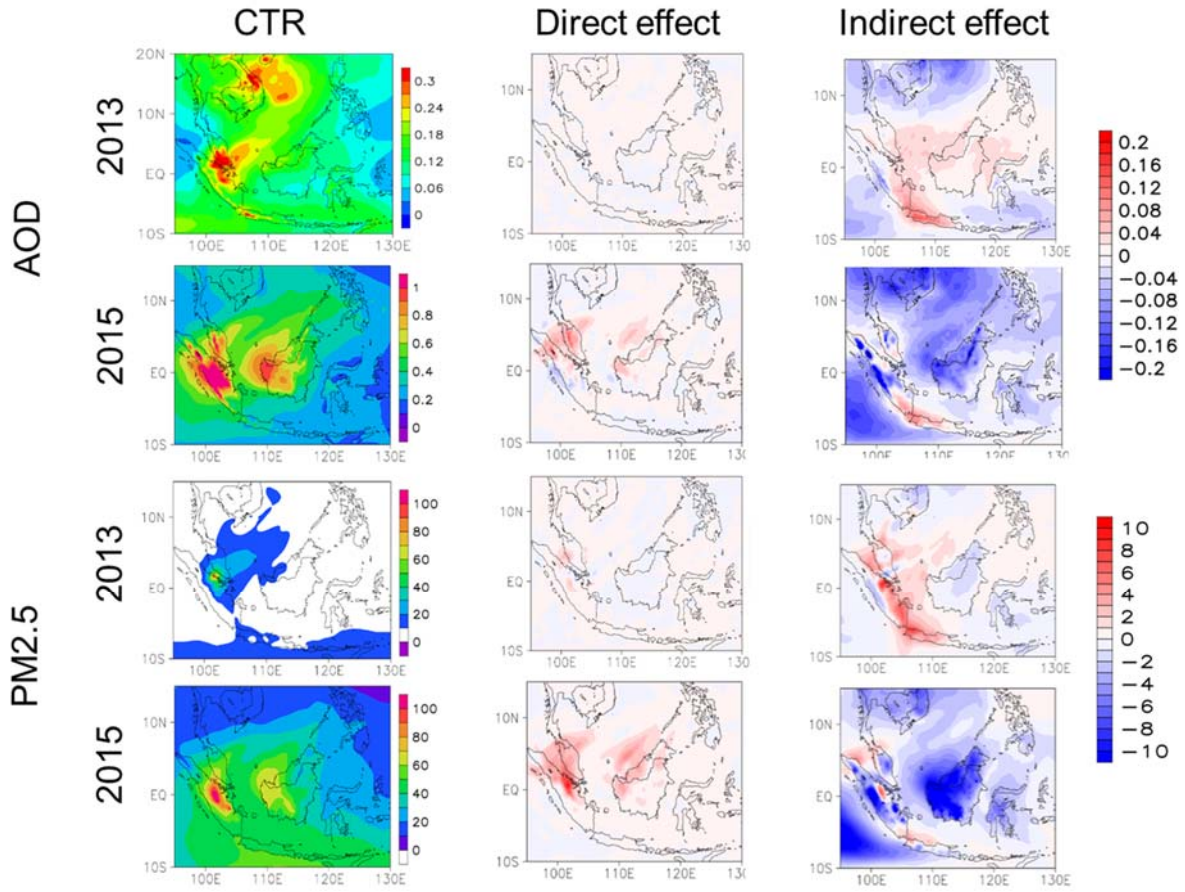

Figure III-32. Simulated aerosol radiative effects (EX1 − CTR), and indirect effects (EX2 – EX1) on monthly mean AOD, $PM_{2.5}$ over Maritime continent in June, 2013 and September, 2015.

In the aerosol direct effect, the effect of aerosol interception can reduce the surface shortwave radiation, and cools the surface which results in less upward motion, reducing PBL height. Under those conditions, there is less cloud and precipitation expected to generate by model in which the removal mechanism of mass concentration is hardly to occur. In Fig. III-32, due to significant reduction of solar radiation and the PBL height, AOD and $PM_{2.5}$ is highly enhanced during the biomass burning. The reason can be that reduction of the PBL height enhances near-surface $PM_{2.5}$ concentration. Fig. III-33 shows the monthly $PM_{2.5}$ vertical difference in the aerosol direct effect (EX1 – CTR) in the right figure. The figure is plotted by calculating firstly by averaging all time step, followed by the average PM2.5 value on – 5S to 5N latitude, and then subtracting the vertical wind in EX1 to CTR. The y-axis value is the pressure level extending from surface to 20 km and the x-axis is the longitude. The results shows that most of $PM_{2.5}$ is increased from surface up to 4 km above, and concentrated in the biomass burning source region which are from 100 – 105ºE and 110 – 115ºE. The left figure shows the monthly AOD, precipitation, the PBL height (left) values which are calculated firstly by averaging all time step, followed by the average of each variables on – 5ºS to 5ºN latitude, and then subtracting the vertical wind in EX1 to

CTR. The figure shows the value series on longitude from 95 – 130ºE. It can be seen that in the region where the $PM_{2.5}$ is increased, it is associated with the region where the PBL height is decreased. The figure also reveals that the high concentration areas usually goes along with low PBL height regions. Furthermore, the aerosol direct effect reduces the vertical wind transport as shown in the Fig, III-34, less vertical wind is simulated by the model when the aerosol direct effect is taken into account. Due to less vertical wind transported to the upper atmosphere, there is also less cloud as well as precipitation formation suggesting that the removal mechanism of wet deposition in the aerosol direct effect is not much contribution. Because the model suppresses the ventilation process of pollutant and stabilize the near-surface atmosphere which lead to increase not only AOD, $PM_{2.5}$ but also other gas pollutants.

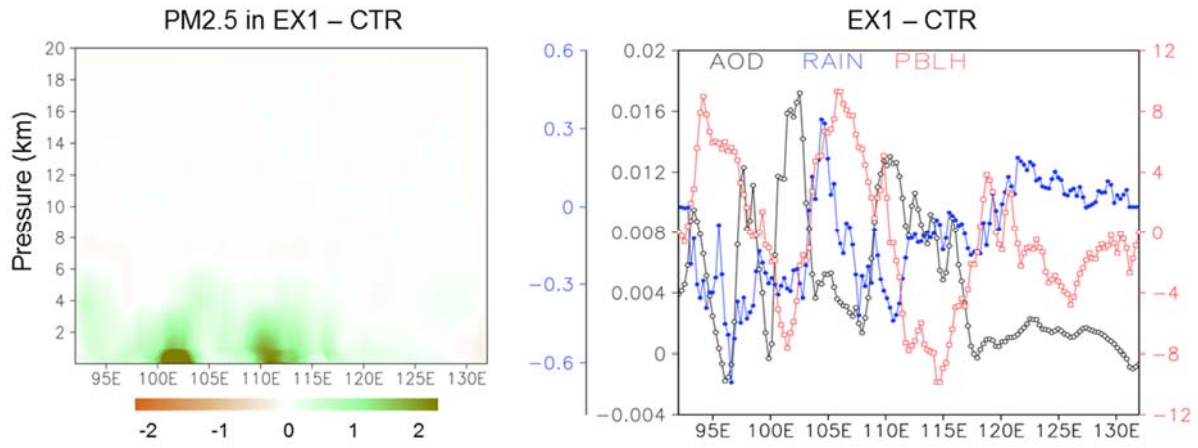

Figure III-33. Monthly $PM_{2.5}$ vertical difference in the aerosol direct effect (EX1 – CTR) (right) and monthly AOD, rain, the PBLH (left) averaged on – 5ºS to 5ºN latitude

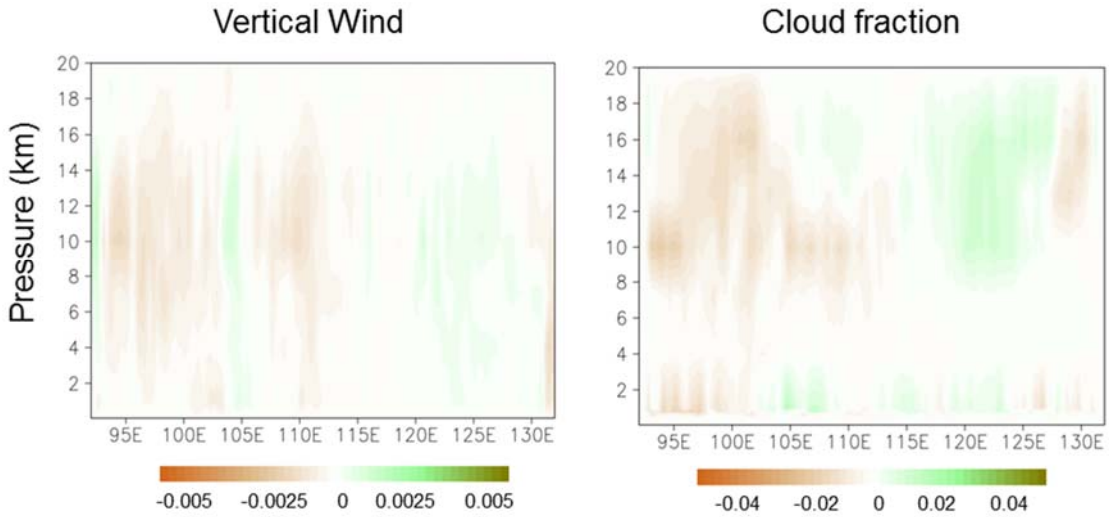

Figure III-34. Monthly vertical wind profile (right) and cloud fraction (left) in the aerosol direct effect (EX1 – CTR) averaged on – 5ºS to 5ºN latitude

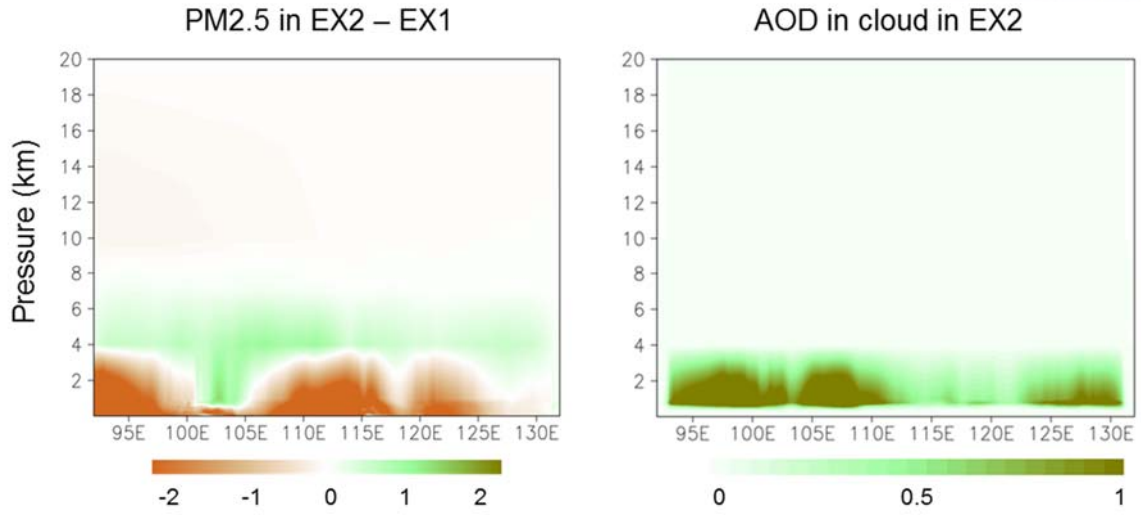

Figure III-35. Monthly $PM_{2.5}$ vertical wind profile (right) and monthly AOD, rain, the PBLH (left) in the aerosol indirect effect averaged on – 5°S to 5°N latitude

Decrease of $PM_{2.5}$ and AOD in EX2 simulation can be mostly due to three reasons. Firstly, the cloud droplet number is mainly due to a simulated atmospheric aerosol number rather than what is prescribed when aerosol indirect effect takes into account in the model. After activation, this process allows interstitial air-borne aerosols to become cloud-borne aerosols. Therefore, air-borne aerosols are decreased in EX2 simulation when the aerosol indirect effect included. Secondly, increased precipitation can also reduce the air-borne particles. The Wesely et al. (2004) parameterization scheme for in and below-cloud aerosol wet removal is included in to the model simulation in the aerosol indirect effect whereas this option do not turn on in the aerosol direct effect. The aerosol wet removal mechanism is considered to be irreversible and the aerosol re-suspension is not happened. Therefore, there will be more aerosols loss in case of including aerosol indirect effect. As shown in Fig. 35, the right figure presents the vertical $PM_{2.5}$ difference in the EX2 and CTR simulation and the left figure presents the amount of aerosol loss into the cloud. It can be seen that most of the negative $PM_{2.5}$ increment is associated with the high incensement of AOD in cloud. In general, the shortwave radiation flux, near-surface temperature and wind speed is reduced when aerosol direct effect is included in model simulation. Due to reduction in those meteorological variables, the atmospheric convection is further weaken leading to a lower stable atmosphere. Having low PHL height and less vertical transport, primary gas pollutants such as NOX, CO, O_3, AOD and $PM_{2.5}$ are increased. However, including the aerosol indirect effect leads to reduce AOD and $PM_{2.5}$, it can be suggested that the wet removal mechanism is activated leading large aerosol removal due to wet deposition and the aerosol transition from airborne aerosol to cloud-borne aerosol in which aerosol losses in cloud irreversibly.

IV. Conclusion

In Southeastern Asia specially Java, Sumatra, Borneo regions, AOD varies annually with the main source of biomass burning which usually peaks during JJASO periods and diminish due to the Asia monsoon with large precipitation amount. The seasonally cycles indicates that AOD has strong positive correlation with Fire, and negative correlation with Precipitation. Inter-annual variability shows that AOD has strong relationship with ENSO which is high during El-Nino and low during La-Nina. Furthermore, analysis of MERRA-2 data reveals that AOD in the region is not only come from organic carbon, but from sulfate as high proportion. Other AOD components such as black carbon, dust and sea salt contributes to the total AOD. However, there is only 60% of AOD components is due to OC quantitatively during the high biomass burning. This indicates that sulfate is mainly contributing from a background source. We further analyzed the correlation of organic carbon, black carbon, sulfate, sea salt, AOD to the El Niño Southern Oscillation. The results show that each AOD components has highly positively correlated with ENSO except for the dust. During the biomass burning the amount of black carbon is 5-6 times smaller than organic carbon quantitatively. The dust component mainly transports from other regions, whereas sea salt and sulfate is in the background source. In order to investigate the impacts of aerosol effect on regional climate, the coupled Weather Research and Forecasting/Chemistry (WRF-Chem) model is used to simulate the severe winter haze conditions over Maritime continent during a haze episode in June 2013 and September 2015 those selected months are standing for a fire during La-nina and El-nino years. The first two primary simulations are that simulations with and without the fire inventory. The results shows that with the fire inventory, model shows better AOD simulated results compared to the without case. Although the domain-averaged AOD value in the without case relatively equal to with fire case, it only come from other sources such as anthropogenic, biogenic emission sources. The spatial distribution of the without fire case shows no signal of the biomass burning (fire) in the simulation. We further analyzed the impact of using FDDA in AOD simulation by carrying out the two simulations with and without FDDA, the simulation with FDDA showed better meteorological variable simulated (e.g. wind) however, it is less accuracy in case of producing the AOD value and significantly underestimated the average precipitation. On the other hand, model simulation without FDDA shows high correlation with AOD value retrieved from MERRA-2 and MODIS, although still shows model bias. Compared model single grid point to AERONET, it shows good model's capability in capture the temporal evolution of the AOD and high correlation to MODIS and AERONET which indicates model qualifies to further examine the impact of aerosol through direct and indirect effect. In the next step, three simulation scenarios including the simulation of no aerosol effect, aerosol direct and indirect effects without using the FDDA are carried out. Even though model still underestimates AOD in both simulation cases for 2013 and 2015, the simulated domain-averaged value of AOD generally have high correlation with MODIS and MERRA-2,

especially in the 2013 case. Comparisons between different simulations shows that both aerosol direct and indirect effects reduce the surface shortwave radiation flux, 10 m wind speed and the PBL height. The results show both direct and indirect aerosol effect has impacts on regional climate. Reducing the PBL height and stabilizing lower atmosphere, the aerosol direct effect enhances near-surface concentrations of atmospheric primary trace gases such as NOx, CO, SO_2, and O_3. Unlike in the above discussion that both aerosol direct and indirect have impacted on the regional meteorology, the aerosol indirect has small influence on gas pollutants. A large aerosol impact on gas pollutant (e.g. CO, NOx, and Ozone) is more dominant by aerosol indirect effect. Biomass burning is a long-day haze event phenomenon, therefore, emissions of short-lived components such CO (~60days), NOx (0.5-2 days) mostly condensed at source. Ozone has generally longer atmospheric resident time (100 days), slightly smaller at source, but larger downwind (e.g. CO, NOX, NMVOCs contribution). For AOD and $PM_{2.5}$, in direct effect, more aerosol reduces shortwave radiation at surface led to surface cooling and less upward motion, reduce the PBLH, cloud and rain, which consequently increase AOD. In indirect effect, more aerosol captured in cloud, and the effect of wet scavenging is reduced AOD. Although the direct and indirect feedbacks on aerosol mass concentrations are subject to uncertainties, this work demonstrates the significance of aerosol feedback for real-time air quality forecasting under haze conditions.

V. Reference

Ackerman A. S. , V. Ramanathan, A. J. Heymsfield, E. J. Welton. (2000). Reduction of Tropical Cloudiness by Soot. *Science, 288*, pp. 1042–1047.

Ackerman S. A., Frey R. A., Strabala K. I., Moeller C. C., Menzel W. P., & Gumley L. E. (1998). Discriminating clear sky from clouds with MODIS. *Journal of Geophysical Research: Atmospheres, 103*(D24), 32141-32157

Aditama, T. Y. (2000). Impact of haze from forest fire to respiratory health: Indonesian experience. *Respirology* (5), 169-174.

Adler R. F., Nelkin E. J., Curtis S., David T. B., (2000). Tropical Rainfall Distributions Determined Using TRMM Combined with Other Satellite and Rain Gauge Information. *J. Appl. Meteorol., 39*(2007-2023).

Alam, K. (2014). Aerosol Characteristics and Radiative Forcing during Pre-Monsoon and Post-Monsoon Seasons in an Urban Environment. *Aerosol and Air Quality Research*.

Alam, K., Blaschke, & T Qureshi, S.,. (2011). Monitoring spatio-temporal aerosol patterns over Pakistan based on MODIS, TOMS and MISR satellite data and a HYSPLIT model. *Atmospheric Environment, 45*(27), 4641-4651.

Aouizerats, B., van der Werf, G. R., Balasubramanian, R., & Betha, R. (2015). Importance of transboundary transport of biomass burning emissions to regional air quality in Southeast Asia during a high fire event. *Atmospheric Chemistry and Physics, 15*(1), 363-373.

Barber C.V. (2000). Trial by Fire: Forest Fires and Forestry Policy in Indonesia's Era of Crisis and Reform. World Resource Institute, Washington D.C.

Beljaars, A. C. M. (1994). The parameterization of surface fluxes in large-scale models under free convection. *Quart. J. Roy. Meteor. Soc., 121*(255-270).

Brauer M, H.-H. J. (1998). Fires in Indonesia: crisis and reaction. *Environmental Science & Technology, 32*, 404–407.

Chaboureau, J.-P., E., Pinty, Di Girolamo, Richard, J.-P., Flamant, C. Wulfmeyer, C., P., Kiemle (2011). Long-range transport of Saharan dust and its radiative impact on precipitation forecast: a case study during the Convective and Orographically-induced Precipitation Study (COPS). *Quarterly Journal of the Royal Meteorological Society, 137*(S1), 236-251.

Chang, S.-S., Wang, L.-C., Lin, N.-H., Lee, W.-J., & Chang-Chien (2013). Influence of the Southeast Asian biomass burnings on the atmospheric persistent organic pollutants observed at near sources and receptor site. *Atmospheric Environment, 78*, 184-194.

Cheyne, S. M. (2008). Effects of meteorology, astronomical variables, location and human disturbance on the singing apes: Hylobates albibarbis. *Am J Primatol, 70*(4), 386-392.

Chou, M.-D., M. J. S. (1994). An efficient thermal infrared radiation parametrization for use in general circulation models. *NASA Tech. Memo. 104606, 3*, 85 pp.

Dubovik, O., King, M. D. (2000). A flexible inversion algorithm for retrieval of aerosol optical properties from Sun and sky radiance measurements. *Journal of Geophysical Research: Atmospheres, 105*(D16), 20673-20696.

Emmons, L. K., S., D., Granier, C., Guenther, A., Kinnison, D., Lamarque, J.-F., Pfister, G. G., Laepple, T., Orlando, J., Tie, X., Tyndall, G., Wiedinmyer, C., Hess, P. G., Fillmore, Baughcum, S., L.,Walters, (2010). Description and evaluation of the Model for Ozone and Related chemical Tracers, version 4 (MOZART-4). *Geosci. Model Dev., 3*(43-67).

Engling, G., Balasubramanian, R., He, J., Betha, R (2014). Assessing the regional impact of indonesian biomass burning emissions based on organic molecular tracers and chemical mass balance modeling. *Atmospheric Chemistry and Physics, 14*(15), 8043-8054.

Forkel, R., Grell, G., Werhahn, Peckham, S., J., McKeen, S., Hansen, A. B & Suppan, P. (2012). Effect of aerosol-radiation feedback on regional air quality – A case study with WRF/Chem. *Atmospheric Environment, 53*, 202-211.

Gadde, B., Bonnet, S., Garivait., &S. Menke, C (2009). Air pollutant emissions from rice straw open field burning in India, Thailand and the Philippines. *Environmental Pollution, 157*(5), 1554-

1558.

Gao, M., Yu, M., Wang, Y., Xin, J., Saide, P. E., Wang, Z. Carmichael, G. R., (2016). Modeling study of the 2010 regional haze event in the North China Plain. *Atmospheric Chemistry and Physics, 16*(3), 1673-1691.

Gautam, R., Jantarach, T. Lau, Holben, B. N., Eck, T. F., Janjai, S., W. K. Hsu, N. C., (2013). Characterization of aerosols over the Indochina peninsula from satellite-surface observations during biomass burning pre-monsoon season. *Atmospheric Environment, 78*, 51-59.

Ge, J. M., Q., Huang, Su, J., Fu, J. P. Shi, J. S. Ackerman, T. P., (2010). Dust aerosol optical properties retrieval and radiative forcing over northwestern China during the 2008 China-U.S. joint field experiment. *Journal of Geophysical Research, 115*.

Giglio, L., Christopher O., Ivan. Justice, Csiszar (2006). Global distribution and seasonality of active fires as observed with the Terra and Aqua Moderate Resolution Imaging Spectroradiometer (MODIS) sensors. *Journal of Geophysical Research: Biogeosciences, 111*(G2).

Grell, G. A. D., Dezső. (2002). A generalized approach to parameterizing convection combining ensemble and data assimilation techniques. *Geophysical Research Letters, 29*(14), 38-31-38-34.

Grell, William C. Eder, G. A. P., Rainer McKeen, Steven E. Schmitz, Gregory Skamarock, Stuart A. Frost, Brian. (2005). Fully coupled "online" chemistry within the WRF model. *Atmospheric Environment, 39*(37), 6957-6975.

Guenther, A., Harley, P., Karl, T., Wiedinmyer, C., P. I.,and Geron, C. Palmer, (2006). Estimates of global terrestrial isoprene emissions using MEGAN (Model of Emissions of Gases and Aerosols from Nature. *Atmos. Chem. Phys.,, 6*(3181–3210).

Hansen, M. C., M.,DiMiceli, C., Townshend, J. R. G., DeFries, R. S., Carroll, and Sohlberg, R. (2003). Global percent tree cover at a spatial resolution of 500 meters: first results of the MODIS Vegetation Continuous Fields algorithm. *Earth Interact., 7*(1–15).

Haywood, J., & Boucher, O. (2000). Estimates of the direct and indirect radiative forcing due to tropospheric aerosols: A review. *Reviews of Geophysics, 38*(4), 513-543.

Heil A, G. J. (2001). Smoke-haze pollution: a review of the 1997 episode in Southeast Asia. *Regional Environmental Change, 2*, 24-37.

Holben B. N., I. Jankowiak, P. Buisk, D. Tanre, A. Setzer, E. Vermote, Y. J. Kaufman, J. A. Reagan, T. Nakajima, F. Lavenu, I. Slutsker, and A. Smirnov. (1998). AERONET—A Federated Instrument Network and Data Archive for Aerosol Characterization. *Remote Sensing Environment, 66*(1–16).

Hong, S.-Y., Y. Noh, and J. Dudhia,. (2006). A new vertical diffusion package with explicit treatment of entrainment processes. *Mon. Wea. Rev., 134*(2318–2341).

Huang, K., Tsay, S.-C., Hsu, N. C., Fu, J. S., Gao, Y., Dong, X., & Lam, Y. F. (2013). Impact assessment of biomass burning on air quality in Southeast and East Asia during BASE-ASIA. *Atmospheric Environment, 78*, 291-302.

Ito, A. (2004). Global estimates of biomass burning emissions based on satellite imagery for the year 2000. *Journal of Geophysical Research, 109*(D14).

Janet, N. (1998). Smoke Haze In Southeast Asia: A Predictable Recurrence *Atmospheric Environment, 32*(14/15), pp. 2715-2716.

Jena, C., Kumar, R., Beig, G., Pfister, G. G., Chate, D. M., Ghude, S. D., van der A, R. J. (2015). Inter-comparison of different NOX emission inventories and associated variation in simulated surface ozone in Indian region. *Atmospheric Environment, 117*, 61-73.

Kaufman, Y. J., Remer, L. A., Tanré, D., Chu, A., Vermote, E. F., & Holben, B. N. (1997). Operational remote sensing of tropospheric aerosol over land from EOS moderate resolution imaging spectroradiometer. *Journal of Geophysical Research: Atmospheres, 102*(D14), 17051-17067.

King., W.P. Menzel, M. D. K., S. Platnick, Y.J. Kaufman, B.C. Gao, D. Tanre, S.A. Ackerman, R. Pincus, L.A. Remer, P.A. Hubanks (2003). Cloud and aerosol properties, precipitable water, and profiles of temperature and water vapor from MODIS. *Geosci. Remote Sens., 41*, pp. 442–458.

King, M. D., L. A. Remer, W. P. Menzel, and P. A. Hubanks, Y. J. Kaufman, D. Tanré, S. Platnick, S.

A. Ackerman, B. C. Gao, R. Pincus,. (2003). Cloud, Aerosol and Water Vapor Properties from MODIS. *IEEE Trans. Geosci. Remote Sens, 41*, pp. 442-458.

Kobayashi, H., T., Hoyano, Matsunaga, Komori, D., A., Aoki, M., & Boonyawat, S. (2004). Satellite estimation of photosynthetically active radiation in Southeast Asia: Impacts of smoke and cloud cover. *Journal of Geophysical Research: Atmospheres, 109*(D4).

Lawrence C.C. Koe, John L. McGregor, A. F. A. J., (2001). Investigating the haze transport from 1997 biomass burning in Southeast Asia: its impact upon Singapore. *Atmospheric Environment, 35*(2723-2734).

Levy, R. C., Kleidman, R. G., Ichoku, C., Kahn, Remer, L. A., Mattoo, S., R., & Eck, T. F. (2010). Global evaluation of the Collection 5 MODIS dark-target aerosol products over land. *Atmospheric Chemistry and Physics, 10*(21), 10399-10420.

Lin, N.-H., G.-R., Wang, Maring, M.-C., Sheu, H. B., Yen, S.-H., Liu, G.-R. (2013). An overview of regional experiments on biomass burning aerosols and related pollutants in Southeast Asia: From BASE-ASIA and the Dongsha Experiment to 7-SEAS. *Atmospheric Environment, 78*, 1-19.

Liu, X.-Y., Zhang, Q., Zhang, Y., & He, K.-B. (2016). Application of online-coupled WRF/Chem-MADRID in East Asia: Model evaluation and climatic effects of anthropogenic aerosols. *Atmospheric Environment, 124*, 321-336.

Lohman DJ, B. D., Sodhi NS. (2007). The burning issue. *Science*, 316-376.

LR, C. (2013). Silver lining of Singapore's Haze. *Science, 341*, 342–343.

McCauley, D. J., Mills, M. M., Young, H. S., Dunbar, R. B., Dirzo, R., Desalles, P. A., & Micheli, F. (2012). From wing to wing: the persistence of long ecological interaction chains in less-disturbed ecosystems. *Sci Rep, 2*, 409.

Miller, R. L., Perlwitz, & J. Tegen, I., (2004). Surface radiative forcing by soil dust aerosols and the hydrologic cycle. *Journal of Geophysical Research: Atmospheres, 109*(D4).

Mlawer, E. J., Iacono, M. J., Taubman, S. J., Brown, P. D., & Clough, S. A. (1997). Radiative transfer for inhomogeneous atmospheres: RRTM, a validated correlated-k model for the longwave. *Journal of Geophysical Research: Atmospheres, 102*(D14), 16663-16682.

Morrison, H., Tatarskii, V. & Thompson, G., (2009). Impact of Cloud Microphysics on the Development of Trailing Stratiform Precipitation in a Simulated Squall Line: Comparison of One- and Two-Moment Schemes. *Monthly Weather Review, 137*(3), 991-1007.

Mott, J. A., C. J., Kiyu, Mannino, Lee, T. Redd, D. M., Alverson, A., Hashim, J., S. C. (2005). Cardiorespiratory hospitalizations associated with smoke exposure during the 1997, Southeast Asian forest fires. *Int J Hyg Environ Health, 208*(1-2), 75-85.

N, S. (2002). Forest fires, air pollution, and mortality in Southeast Asia. *Demography, 39*, 01-23.

Neu, J. L., & Prather, M. J. (2012). Toward a more physical representation of precipitation scavenging in global chemistry models: cloud overlap and ice physics and their impact on tropospheric ozone. *Atmospheric Chemistry and Physics, 12*(7), 3289-3310.

Okada K, Jensen JB, Makino Y, I. M., Zaizen Y, Gras JL (2001). The mixture state of individual aerosol particles in the 1997 Indonesian haze episode. Aerosol Science, 32, 1269–1279. *Aerosol Science, 32*, 1269–1279.

Paul J. C., A. O. M. (1990). Biomass burning in the Tropics: Impacts on Atmospheric Chemistry and Biogeochemical Cycles. *Science, 250*(1669-1678).

Permadi, D. A., & Kim Oanh, N. T. (2013). Assessment of biomass open burning emissions in Indonesia and potential climate forcing impact. *Atmospheric Environment, 78*, 250-258.

Pfister, G. G., Wiedinmyer, C., Avise, J., Edwards, D. P., Diskin, G. D. Wisthaler, A. Emmons, L. K., (2011). CO source contribution analysis for California during ARCTAS-CARB. *Atmospheric Chemistry and Physics, 11*(15), 7515-7532.

Posa, M. R. C., Wijedasa, L. S., & Corlett, R. T. (2011). Biodiversity and Conservation of Tropical Peat Swamp Forests. *BioScience, 61*(1), 49-57.

Radojevic, M. (2003). Chemistry of forest fires and regional haze with emphasis on Southeast Asia. *Pure and Applied, 160*, 157-187.

Reid, J. S., Holben, B. N., Hyer, E. J., Yokelson, R. J., Zhang, Johnson, R. S., J., Liew, S. C. (2013).

Observing and understanding the Southeast Asian aerosol system by remote sensing: An initial review and analysis for the Seven Southeast Asian Studies (7SEAS) program. *Atmospheric Research, 122*, 403-468.

Remer, L. A., Kaufman, R.G., Eck, Y.J.,Tanré, D., Mattoo, S., Chu, D.A., T.F., Vermote, E., Martines, J.V., Ichoku, C., Levy, R.C., Kleidman, Li, R.R., and Holben, B.N. (2005). The MODIS Aerosol Algorithm, Products, and Validation. *J. Atmos. Sci.,, 62*, 947–973.

S., J. (2005). Air Quality and Infant Mortality during Indonesia's Massive Wildfires in 1997. *Technical Report Number 95, BREAD: Bureau for Research in Economic Analysis of Development, Cambridge, MA*.

Satheesh, S., & Krishnamoorthy, K. (2005). Radiative effects of natural aerosols: A review. *Atmospheric Environment, 39*(11), 2089-2110.

Seinfeld, J. H. C., J.Markowicz, G. R.Arimoto, T. A.Clarke, F. J.Bates, P. B.Shimizu, Y. H.Uno, W. C.Brechtel, A.Shinozuka, J. H.Zhang, X. Y., R.Conant, C. H.Tang, T. S.Cahill, A. D.Doherty, S. J.Flatau, P. J.Huebert, B. J.Kim, K. M.Quinn, P. K.Russell, L. M.Russell, Y.Song, I.Vogelmann, A. M.Weber, R. J.Woo, (2004). ACE-ASIA - Regional climatic and atmospheric chemical effects of Asian dust and pollution. *Bulletin of the American Meteorological Society, 85*(3), 367-+.

Skamarock, W. C., D. M. Barker, W. Wang, J. B. Klemp, J. Dudhia, M. Duda, X.-Y. Huang, D. O. Gill, and J. G. Powers (2008). A description of the Advanced Research WRF version 3. *NCAR Tech. Note NCAR/TN-475+STR*, 125 pp.

SR, A. (2004). Runaway fires, smoke-haze pollution and unnatural disasters in Indonesia. *Geographical Review, 94*, 55-79.

Stanelle, T., Bäumer, D., Vogel, B., Kottmeier, C., & Vogel, H. (2010). Feedback between dust particles and atmospheric processes over West Africa during dust episodes in March 2006 and June 2007. *Atmospheric Chemistry and Physics, 10*(22), 10771-10788.

Sundarambal, P., Tkalich, P., Balasubramanian, R., & He, J. (2010). Impact of biomass burning on ocean water quality in Southeast Asia through atmospheric deposition: field observations. *Atmospheric Chemistry and Physics, 10*(23), 11323-11336.

Tacconi, L., Jotzo, F., & Grafton, R. Q. (2007). Local causes, regional co-operation and global financing for environmental problems: the case of Southeast Asian Haze pollution. *International Environmental Agreements: Politics, Law and Economics, 8*(1), 1-16.

Tacconi, L., & Vayda, A. P. (2006). Slash and burn and fires in Indonesia: A comment. *Ecological Economics, 56*(1), 1-4.

Tanré, D., Herman, M., Kaufman, Y. J., & Mattoo, S. (1997). Remote sensing of aerosol properties over oceans using the MODIS/EOS speCTRal radiances. *Journal of Geophysical Research: Atmospheres, 102*(D14), 16971-16988.

Teller, A., Levin., & Z. Xue, L (2012). The effects of mineral dust particles, aerosol regeneration and ice nucleation parameterizations on clouds and precipitation. *Atmospheric Chemistry and Physics, 12*(19), 9303-9320.

Thompson, G., K. Manning & R. M. Rasmussen (2004). Explicit forecasts of winter precipitation using an improved bulk microphysics scheme. Part I: Description and sensitivity analysis. *Mon. Wea. Rev., 132*, 519-542.

Tompkins, A. M. (2005). Influence of aerosol climatology on forecasts of the African Easterly Jet. *Geophysical Research Letters, 32*(10).

Vasconcelos, S., Graça, Nogueira, E. M., P. M. L. d. A., Oliveira, L. C., Fearnside, P. M., & Figueiredo, E. O. (2013). Forest fires in southwestern Brazilian Amazonia: Estimates of area and potential carbon emissions. *Forest Ecology and Management, 291*, 199-208.

Wang, Y. (2004). Trends in atmospheric haze induced by peat fires in Sumatra Island, Indonesia and El Niño phenomenon from 1973 to 2003. *Geophysical Research Letters, 31*(4).

Wesely, M. L. (1989). Parameterization of surface resistance to gaseous dry deposition in regional-scale numerical models. *Atmos. Environ.,, 23*(1293–1304).

Wiedinmyer, C., Yokelson, R. J., Akagi, S. K., Emmons, L. K., Orlando, J. J., Al-Saadi, J. A., & Soja, A. J. (2011). The Fire INventory from NCAR (FINN): a high resolution global model to

estimate the emissions from open burning. *Geoscientific Model Development, 4*(3), 625-641.

Yule, C. M. (2008). Loss of biodiversity and ecosystem functioning in Indo-Malayan peat swamp forests. *Biodiversity and Conservation, 19*(2), 393-409.

Zaveri, R. A., Peters, L. K. Easter, R. C., & Fast, J. D (2008). Model for Simulating Aerosol Interactions and Chemistry (MOSAIC). *Journal of Geophysical Research, 113*(D13).

Zhang, B., Hao, & J. Wang, Y., (2015). Simulating aerosol–radiation–cloud feedbacks on meteorology and air quality over eastern China under severe haze conditionsin winter. *Atmospheric Chemistry and Physics, 15*(5), 2387-2404.

Zhao, C., Ruby Leung, L., Liu, X., & Hagos, S. (2011). Radiative impact of mineral dust on monsoon precipitation variability over West Africa. *Atmospheric Chemistry and Physics, 11*(5), 1879-1893.